Long noncoding RNA *AVAN* promotes antiviral innate immunity by interacting with TRIM25 and enhancing the transcription of FOXO3a

Chengcai Lai[1,7,#], Lihui Liu[2,3,#], Qinghua Liu[2,3,4,#], Sijie Cheng[5,#], Keyu Wang[1,6], Lingna Zhao[1], Min Xia[1], Cheng Wang[6], Hongjing Gu[1], Yueqiang Duan[1], Zhongpeng Zhao[1], Lili Zhang[2,3,8], Ziyang Liu[2,3,8], Jianjun Luo[2,3], Jianxun Song[9], Penghui Yang[1,5,*], Runsheng Chen[2,3,6,*], Xiliang Wang[1,*]

[1] State Key Laboratory of Pathogens and Biosecurity, Beijing Institute of Microbiology and Epidemiology, Beijing 100071, China

[2] Key Laboratory of RNA Biology, Institute of Biophysics, Chinese Academy of Sciences, Beijing 100101, China

[3] Beijing Key Laboratory of Noncoding RNA, Institute of Biophysics, Chinese Academy of Sciences, Beijing 100101, China

[4] Guangdong Geneway Decoding Bio-Tech Co. Ltd, Foshan 528316, China

[5] Beijing 302 Hospital, Beijing 100039, China

[6] Chinese PLA General Hospital, Beijing 100853, China

[7] NO.95316 Troops of PLA, Guangzhou, 510900, China

[8] University of Chinese Academy of Sciences, Beijing, 100049, China

[9] Microbial pathogenesis and Immunology, Texas A&M University College of Medicine, Hershey, TX 77843, USA

[#] These authors contributed equally to this work.

[*] Correspondence author: X.W. (xiliangw@126.com), C.R. (crs@sun5.ibp.ac.cn), or Y. P.

(ypenghuiamms@hotmail.com)

Abstract

Accumulating evidence has shown that long noncoding RNAs (lncRNAs) are involved in several biological processes, including immune responses. However, the role of lncRNAs in antiviral innate immune responses remains largely unexplored. Here, we identify an uncharacterized human lncRNA, antivirus and activate neutrophil (*AVAN*), that is significantly up-regulated upon virus infection. Mechanistically, nuclear lncRNA-*AVAN* positively regulates the transcription of forkhead box O3A (FOXO3a) *in cis* by associating with its promoter and inducing chromatin remodeling to promote neutrophil chemotaxis. Furthermore, we also found that cytoplasmic lncRNA-*AVAN* directly binds tripartite motif containing 25 (TRIM25) and enhances the association of TRIM25 and Retinoic acid inducible gene-1 proteins (RIG-I) and the ubiquitylation of RIG-I, thereby promoting TRIM25- and RIG-I-mediated antiviral innate immune signaling. Collectively, these findings highlight the potential clinical implications of lncRNA-*AVAN* as a key positive regulator of the antiviral innate immune response and a promising target for developing broad antiviral therapeutics.

Keywords: long noncoding RNA, *AVAN*, virus immunity, FOXO3a, TRIM25

Introduction

Long noncoding RNAs (lncRNAs), a large class of noncoding RNAs with no or limited coding potential, are defined as functional RNAs that participate in a wide range of biological processes, including cell and organ development, X-chromosome inactivation, tumor proliferation, genomic imprinting, and stem cell self-renewal (1-10). lncRNAs are also reportedly involved in innate and adaptive immune responses, such as immune cell proliferation and cytokine production (11-14). Previous studies have shown that lncRNAs exert their roles in regulating chromatin accessibility, mRNA stability and protein activity by interacting with chromatin DNA, mRNAs or proteins (15-18). With the discovery and characterization of an increasing number of lncRNAs, several mechanisms of these lncRNAs in virus-host interactions have been elucidated (19), however, many others remain uncharacterized.

Influenza A virus (IAV) is a leading cause of respiratory-related morbidity and mortality, posing a substantial threat to global health (20). However, some mechanisms underlying IAV-host interactions remain unclear. Neutrophils provide one of the early lines of innate immunity and defense against invading microorganisms, which contribute to the fine regulation of the inflammatory and antiviral immune responses (21-23). Increasing evidence suggests that neutrophils are also prominent components of the inflammatory and immune responses during virus infection. Neutrophils are rapidly recruited to sites of infection during the innate immune response to IAV (24-26). In addition, neutrophils can produce and release a large variety of cytokines and chemokines (22), which enables them to significantly influence antiviral defense (27). During virus infection, chemokines play a crucial role in neutrophil

63 activation and chemotaxis (28). However, how lncRNA functions in this process is largely
64 unknown.

65 Intracellular RIG-I-like receptors (RLRs), namely, RIG-I, MDA5, and LGP2, are
66 well-defined single-stranded viral RNA sensors that play a pivotal role in host antiviral
67 activity by initializing the rapid production of type I interferons (IFN) and cytokines (29).
68 RIG-I is a key sensor of paramyxoviruses, influenza virus, hepatitis C virus, and Japanese
69 encephalitis virus (30). The binding of viral RNA to the RIG-I C-terminal regulatory domain
70 results in a conformational change that, in turn, enables RIG-I binding to the signal adaptor
71 MAVS (also called VISA, IPS-1, or CARDIF) through N-terminal caspase recruitment
72 domains (CARDs). Such binding enhances the phosphorylation of IRF3 and eventually leads
73 to the production of type I IFN and inflammatory cytokines (31). However, little is known
74 about the roles of lncRNAs in IAV-infected patients or the mechanisms of lncRNA activity
75 and host antiviral immune responses.

76 In this study, we profile the lncRNAs of IAV-infected patient neutrophils and identify a
77 human lncRNA, designated *AVAN*, which plays a critical role in anti-IAV infection.
78 Functional experiments demonstrate that *AVAN* up-regulates FOXO3a expression to promote
79 neutrophil chemotaxis and recruitment. In addition, *AVAN* enhances the activation of the
80 RIG-I-mediated antiviral response by directly binding to TRIM25. These results show that an
81 unannotated lncRNA, *AVAN*, functions to maintain innate immune homeostasis of antiviral
82 immunity during IAV infection.

Results

LncRNA expression is regulated by the influenza A (H7N9) virus in human neutrophils.

Neutrophils, the prototypic cells of the innate immune system, are reported to play a pivotal role in the innate immune response to IAV (21-23). To explore the roles of host lncRNAs during IAV infection, we profiled whole transcriptional alterations using RNA-Seq in neutrophil samples from patients infected with IAV in the acute stage and their matched recovery-stage samples (GSE108807). We identified a total of 404 differentially expressed protein-coding genes (FC>2, $p<0.05$), including 234 up-regulated and 170 down-regulated genes, in each patient sample (Fig S1). The differentially expressed genes were strongly associated with the immune response, inflammatory response and innate immune response according to Gene ontology (GO) analysis (Fig 1A). We then mapped the detected lncRNAs to the human genome (UCSC version hg19) and the NONCODE V3.0 database and found an average of 240 up-regulated (range from 164 to 357) and 193 down-regulated (range from 158 to 257) novel lncRNAs in acute-stage influenza patients compared with their recovery-stage counterparts (FC>2, $p<0.05$) and subjected them to a cluster analysis (Fig 1B). To investigate the association between lncRNAs and IAV infection, *in silico* analysis identified 26 novel lncRNAs candidates with notably aberrant expression (Fig 1C). To confirm the expression of these lncRNAs, we separated the neutrophils and monocytes from healthy volunteers and infected the cells with IAV for 12 h and found that XLOC_040025 (*AVAN*) was most significantly up-regulated after IAV challenge (Fig 1D, E). We also infected human alveolar epithelial cells (A549) with IAV and measured the expression of the 26 lncRNAs and found that *AVAN* was most strongly up-regulated after IAV infection (Fig 1F).

105

106 **_AVAN_ is preferentially up-regulated following virus infection**

107 We then performed qRT-PCR to quantify *AVAN* expression in the RNA-Seq samples and
108 found that the results were consistent with the RNA-Seq data (Fig S2A). Thus, *AVAN* was
109 chosen for subsequent investigation. To further confirm the expression of *AVAN* in
110 IAV-infected patients, we collected blood samples from 63 additional IAV-positive patients
111 and measured the expression of *AVAN*, which was significantly up-regulated in the neutrophils
112 of these patients (Fig 2A; Table S1). Similarly, *AVAN* was up-regulated in A549 cells after
113 infection with multiple sub-strains of IAV and several other viruses, including Sendai virus
114 (SeV) and respiratory syncytial virus (RSV) (Fig 2B). Moreover, *AVAN* expression was
115 significantly up-regulated upon IAV challenge in a time- and dose-dependent manner in A549
116 cells (Fig 2C, D). Moreover, *AVAN* expression was also significantly up-regulated in a time-
117 and dose-dependent manner in the human promyelocytic leukemia cell line (HL60), which is
118 often a substitute for neutrophils, upon IAV challenge (Fig S2B, C). Subcellular fractionation
119 followed by qRT-PCR in IAV-infected A549 cells revealed that the amount of *AVAN* localized
120 in the cytoplasm was nearly as same as the one in nucleus (Fig 2E, Fig S2D). Besides, we
121 performed RNA fluorescence *in situ* hybridization (RNA-FISH) with two specific probes in
122 IAV-uninfected and –infected A549 cells and found that *AVAN* localized in the cytoplasm and
123 nucleus were almost the same abundance (Fig 2F). In addition, we constructed competitive
124 association FISH to display the specific distribution of *AVAN*. When adding free
125 labeling-probes, the fluorescent dye from biotin labeling-probes was weaken (Fig S2E). *AVAN*
126 exhibits no protein-coding potential according to ORF finder (32) and the coding potential

127 calculator (33) (Fig S2F). Only one transcript variant (approximately 500 nt) of *AVAN* was
128 found in A549 cells, and it was found to be up-regulated upon IAV infection using northern
129 blot analysis (Fig 2G). The exact transcript length (517 nt) of *AVAN* was confirmed by 5' and
130 3' RACE (Table S2), which revealed that *AVAN* is polyadenylated (Fig S2G). Taken together,
131 lncRNA expression profiling of patient neutrophils during IAV infection identified a novel
132 *AVAN* that was preferentially up-regulated in IAV-infected cell lines and patient neutrophils
133 upon virus infection.
134
135 **_AVAN_ is essential for antiviral immune responses and neutrophil chemotaxis during IAV**
136 **infection**
137 To evaluate the potential function of *AVAN*, we next analyzed the related gene
138 coexpression networks from the sequencing data and performed gene set enrichment analysis
139 (GSEA). Influenza viral RNA transcription and replication were negatively related to *AVAN*
140 (Fig S3, Table S3-S8), suggesting that *AVAN* participates in innate antiviral immunity. To
141 identify the functions of *AVAN*, we generated *AVAN*-overexpressing A549 cells (Fig 3A) and
142 found that viral replication was strongly inhibited (Fig 3B). In contrast, virus titer was
143 up-regulated following *AVAN* knockdown with two specific siRNAs (Fig 3H, I), indicating
144 that *AVAN* enhances the regulation of antiviral immune responses.
145 Innate immunity provides the first line of defense against invading pathogens. The
146 recognition of invading virus by pathogen-recognition receptors activates the innate immune
147 system, resulting in the production of type I IFNs (IFN-α and IFN-β) and eliciting antiviral
148 responses (34-36). Thus, we assessed whether *AVAN* regulates virus-induced type I IFN

149 production. The results of qRT-PCR indicate that *AVAN* overexpression increased IFN-α and
150 IFN-β transcript levels upon IAV infection compared with those of the control vector (Fig 3C).
151 To confirm this result, we performed ELISA to measure IFN-α and IFN-β protein expression
152 and found that IFN-α and IFN-β were strongly up-regulated in *AVAN*-overexpressing A549
153 cells during IAV infection (Fig 3D). Conversely, these phenomena were abolished by
154 knocking down *AVAN* (Fig 3J, K).

155 The above GSEA data and GO analysis showed that the genes related to *AVAN* were also
156 significantly enriched in chemotaxis and immune cell activation (Fig S4A, Table S9, S10), the
157 main components of innate immune responses. To explore the role of *AVAN* in chemotaxis, we
158 collected culture supernatants of *AVAN*-overexpressing A549cells and performed neutrophil
159 transwell assays, which revealed that *AVAN* overexpression significantly up-regulated
160 neutrophil chemotaxis during IAV infection (Fig 3E). These phenomena were disrupted by
161 knocking down *AVAN* (Fig 3L). The chemokines interleukin-8 (CXCL8, IL-8) is potent
162 neutrophil chemoattractant (37) and is released by a variety of lung cells, including
163 macrophages and epithelial cells as well as neutrophils themselves (38). IL-8 primarily
164 attracts neutrophils and induces them to release lysosomal enzymes, triggering the respiratory
165 burst and increasing the expression of adhesion molecules on the cell surface (39). IL-8 is the
166 primary cytokine involved in the recruitment of neutrophils to the site of damage or infection
167 and plays a crucial role in acute inflammation by recruiting and mediating neutrophils and
168 other cells (40). Thus, we determine whether *AVAN* altered IL-8 expression in A549 cells.
169 *AVAN* overexpression increased IL-8 transcript and protein levels upon IAV infection
170 compared with those of the control vector (Fig 3F, G); this was abolished upon *AVAN*

knockdown (Fig 3M, N). To verify our hypothesis, we next overexpressed or knocked down *AVAN* in HL60 cells (Fig S4C, E) and infected them with IAV. The cell samples were harvested at the indicated times, and transcript and protein levels of IL-8 were measured. The results from HL60 cells were consistent with those obtained in A549 cells (Fig S4D, F). Collectively, these data indicate that lncRNA-*AVAN* plays a vital role in antiviral responses by positively regulating type I IFN induction and neutrophil chemotaxis.

AVAN up-regulates ISG and chemokine expression

To verify the global influence of *AVAN* during virus infection and to gain further insight into *AVAN* activity, we performed cellular transcriptome profiling on A549 cells using cDNA microarrays and found that *AVAN* overexpression altered the expression of 81 genes after 14 h of BJ501 infection compared with control cells (Fig 4A, Table S11). Most of these divergent genes were associated with antiviral innate immune responses and inflammatory diseases according to Reactome pathway analysis (Fig 4B) and FunDO diseases analysis (Fig S5). Notably, genes associated with immune system IFN signaling and cytokine signaling were markedly up-regulated in cells with ectopic *AVAN* expression compared with control cells, including chemokines and ISGs (IFN stimulated genes) (Fig 4C). These significantly up-regulated genes, including MX1, ISG15, IFIT2, OASL, IFIM3, TNFAIP3, CXCL2 and CCL5, were confirmed by qRT-PCR (Fig 4D). These data again reveal that *AVAN* strongly participates in antiviral innate immune processes and neutrophil chemotaxis.

AVAN triggers FOXO3a expression in the nucleus to enhance neutrophil chemotaxis

193 Recent studies have shown that divergent lncRNAs can positively regulate the
194 transcription of nearby genes through chromatin remodeling (4,41-45). The genomic location
195 of *AVAN* suggested that it was divergently transcribed from a position 500-bp upstream of the
196 FOXO3a gene (Fig S2G). Interestingly, mRNA array data revealed that FOXO3a is
197 significantly up-regulated following *AVAN* overexpression during IAV infection (Fig 4C). To
198 investigate the role of *AVAN* in FOXO3a expression, we measured the abundances of
199 FOXO3a after overexpressing or knocking down *AVAN* in A549 and HL60 cell lines. The
200 overexpression of *AVAN* up-regulated FOXO3a transcription in A549 cells, consistent with its
201 role in enhancing FOXO3a protein expression (Fig 5A; Fig S6A left). Conversely, knocking
202 down *AVAN* down-regulated FOXO3a transcription and protein expression (Fig 5B; Fig S6A
203 right). In addition, the results in HL60 were consistent with these observed in A549 cells (Fig
204 S6B).

205 The association of *AVAN* with FOXO3a expression and the subcellular localization of
206 *AVAN* in both the cytoplasm and nucleus (Fig 2E, F) prompted us to test whether *AVAN*
207 interacts with the FOXO3a promoter. To this end, we conducted chromatin isolation by RNA
208 purification (ChIRP) using antisense oligoes against *AVAN* followed by qPCR in BJ501
209 -uninfected and -infected A549 cells and found that *AVAN* bound to sequences upstream of
210 FOXO3a (Fig 5C, D, E). We further verified the potential role of *AVAN* in modulating
211 chromatin modifications at the FOXO3a promoter region. Chromatin immunoprecipitation
212 **(**ChIP)-qPCR revealed that ectopic *AVAN* expression increased Pol II binding, as well as
213 H3K4me3 and H3K27ac levels, at the *AVAN*-coated FOXO3a promoter in virus infected A549
214 cell (Fig 5F, G, H) and uninfected A549 cell (Fig S6D, E, F). In contrast, knocking down

215 *AVAN* decreased Pol II binding and H3K4me3 and H3K27ac accumulation (Fig 5I, J, K; Fig
216 S6G, H, I).

217 Chemokines were markedly up-regulated in cells with ectopic *AVAN* expression (Fig 4C).
218 A previous study reported that FOXO3a can regulate chemokine expression (46). To further
219 investigate whether *AVAN*-promoted chemokines expression is associated with FOXO3a, we
220 measured IL-8 expression in FOXO3a overexpressing A549 cells. Ectopic FOXO3a
221 expression significantly promoted IL-8 expression and neutrophil chemotaxis during IAV
222 infection (Fig 5L, N; Fig S6J). In contrast, knocking down FOXO3a decreased IL-8
223 expression and neutrophil chemotaxis during IAV infection (Fig 5M, O; Fig S6K). In addition,
224 we knocked down FOXO3a in *AVAN*-overexpressing A549 cells and found that knockdown
225 abrogated *AVAN*-induced effects on IL-8 expression during IAV infection (Fig 5P). These data
226 provide evidence that *AVAN* plays a critical role in regulating FOXO3a expression *in cis* by
227 associating with the FOXO3a promoter and performing chromatin remodeling, which
228 additionally increased IL-8 and neutrophil chemotaxis.

229

230 **_AVAN_ direct binds to TRIM25 and enhances the TRIM25-mediated activation of RIG-I**
231 **signaling**

232 Previous experiments demonstrated that *AVAN* is located in the cytoplasm (Fig 2E, 2F).
233 To investigate the molecular mechanism of *AVAN* in the cytoplasm, RNA pull-down assays
234 using biotin-labeled *AVAN* or *AVAN* antisense control followed by mass spectrometry (MS)
235 analysis were performed. The E3 ubiquitin ligase TRIM25, an RNA-binding protein, was
236 found to bind *AVAN* in IAV-infected A549 cells compared with the *AVAN* antisense control

(Fig 6A). This result was confirmed by *AVAN* RNA pull-down western blot experiments (Fig 6B). Besides, ChIRP followed by western blot revealed that *AVAN*-specific probes could pull down TRIM25 while LacZ couldn't (Fig 6C). To validate the interaction between AVAN and TRIM25, we immunoprecipitated TRIM25 from IAV-infected A549 cells and quantified the protein-bound *AVAN*. Significantly higher levels of *AVAN* were detected with exogenous (Fig 6D) and endogenous (Fig 6E) TRIM25 immunoprecipitation than with the isotype immunoglobulin G (IgG) control. Furthermore, we constructed Flag-tagged TRIM25 truncated proteins containing the SPRY domain, B box/central coiled-coil domain (CCD), or RING domain and performed *AVAN* RNA pull-down western blot experiments. The results showed that only the B box/central CCD domain was involved in the *AVAN*-TRIM25 association (Fig 6F). Furthermore, to explore the TRIM25 binding site on AVAN RNA, three truncated probes from AVAN were used for RNA pull-down assay. The result indicated that the TRIM25-binding activity mapped between nucleotides 1 and 200 (Fig 6G). Together, these findings indicate that *AVAN* physically interacts with TRIM25 and that the B box/central CCD of TRIM25 and 1-200nt of AVA*N* contribute to this association.

To test whether *AVAN* enhances the IFN-mediated antiviral innate immune response through TRIM25 and RIG-I signaling, we knocked down endogenous TRIM25 in HEK-293T cells and observed a markedly reduced effect of ectopic *AVAN* expression on the activation of IFNB1-responsive reporters in the context of IAV infection (Fig S7A). RIG-I is polyubiquitinated by TRIM25, which attaches K63-linked polyubiquitin to the sensor (47), Previous study showed that a stabilization of TRIM25-RIG-I interaction is important for a sustained antiviral IFN response (48). We next examined the effect of *AVAN* on the interaction

between TRIM25 and RIG-I. We found that ectopically expressing *AVAN* markedly enhanced the association between TRIM25 and RIG-I upon IAV infection (Fig 6H). Additionally, different fragments of *AVAN* were overexpressed in A549. We observed that P1(1-200nt) could enhance the association between TRIM25 and RIG-I, as full-length *AVAN*, while fragment P2+P3 (201-517nt) couldn't (Fig S7B). Moreover, endogenous or exogenous RIG-I ubiquitylation was significantly increased in *AVAN*-overexpressing cells in the context of IAV infection compared with the control vector (Fig 6I, J). Furthermore, we explored the impact of altered *AVAN* levels on RIG-I signaling. Total RIG-I protein levels did not differ significantly between *AVAN*-overexpressing and control cells. However, *AVAN* overexpression increased TBK1 and IRF3 phosphorylation upon IAV infection (Fig 6K, left). In contrast, *AVAN* knockdown abolished these changes (Fig 6K, right). To test whether AVAN enhances the IFN-mediated antiviral innate immune response through TRIM25 and RIG-I signaling, we performed qPCR analysis measuring IFN-alpha/beta upon AVAN transfection, and then individually knock down RIG-I or TRIM25. The results showed that knock down RIG-I or TRIM25 abrogated AVAN-induced effects on IFN-alpha/beta expression during IAV infection (Fig 6L, M, Fig S7C, D). Together, these data show that *AVAN* can enhance the interaction between TRIM25 and RIG-I and the ubiquitylation of RIG-I in the cytoplasm. Thus, we conclude that *AVAN* promotes TRIM25- and RIG-I-mediated antiviral innate immune signaling.

AVAN protects mice from influenza A infection _in vivo_

To further investigate the *in vivo* effect of *AVAN* on IAV pathogenesis, we constructed an

281 *AVAN*-containing AAV2/9 vector and a control vector, which were then delivered into
282 4-week-old C57L/B6 mice via intranasal (i.n.) administration. We found that *AVAN* was
283 ectopically expressed in the lung of AAV2/9-*AVAN* treated mice (Fig 7A). Strikingly, after
284 BJ501 infection, the groups pretreated with AAV2/9-*AVAN* exhibited significantly increased
285 survival rates and reduced body weight loss at 10 days post-infection compared with the
286 control group (Fig 7B, C). Furthermore, lung edema, measured as the wet-to-dry ratio of
287 whole lung, was ameliorated (Fig 7D), and improved lung histopathology was observed in
288 infected mice pretreated with AAV2/9-*AVAN* (Fig 7E, F). Moreover, the virus titer from the
289 lungs of infected mice was also significantly reduced in AAV2/9-*AVAN*-treated mice
290 compared with that in control mice (Fig 7G, H). Although *AVAN* triggers FOXO3a expression
291 in the nucleus to enhance neutrophil chemotaxis *in vitro*, we did not observe that *AVAN*
292 promotes FOXO3a expression *in vivo* (data not shown). This finding may result from the low
293 conservation of *AVAN* between humans and mice. Consistent with the association in human,
294 we found that *AVAN* also bind to rodent Trim25 through RNA pull-down using mouse tissue
295 (Fig 7I). In addition, AAV2/9-*AVAN* promote type I IFN expression *in vivo* (Fig 7J). Taken
296 together, these observations indicate that *AVAN* can ameliorate IAV-induced acute lung injury
297 *in vivo* and protect mice from IAV infection.
298

Discussion

Recently, increasing evidence supports the importance of lncRNAs in host-virus interactions, and lncRNAs are an emerging paradigm in the regulation of innate immune responses. Previous studies have described several lncRNAs that are differentially expressed during viral infection, including in severe acute respiratory syndrome coronavirus (SARS-CoV)-infected mice, IAV-infected human lung cells and enterovirus 71 (EV71)-infected rhabdomyosarcoma (RD) cells (49-51). However, little is known about the lncRNA profile of influenza patients. In this study, we profiled the transcriptome of neutrophils isolated from IAV-infected patients via RNA-Seq technology for the first time. Through a comprehensive analysis of these data, we identified 404 differentially expressed mRNAs and 433 differentially expressed noncoding RNAs in neutrophils of influenza patients. Among these highly expressed genes, we found an lncRNA named *AVAN* that plays a pivotal role in antiviral responses.

Several studies have shown that differentially expressed lncRNAs function as negative or positive regulators in various critical steps of the antiviral response (52). For example, BISPR lncRNA can regulate the antiviral IFN response through the induction of the expression of the genomically neighboring gene BST2 *in cis*. Another IAV-associated intronic antisense lncRNA, negative regulator of antiviral response (NRAV), modulates antiviral responses by suppressing ISG transcription via altered histone modifications (53). A recent study show that lnc-Lsm3b can compete with viral RNAs in the binding of RIG-I monomers and involve in RIG-I-mediated antiviral response (54). In contrast, Herein, our data displayed that *AVAN* acts as a positive regulator in the antivirus response through two different mechanisms. In one

hand, cytoplasmic lncRNA-AVAN directly binds TRIM25 and enhances the association of TRIM25 and RIG-I and the ubiquitylation of RIG-I, thereby promoting TRIM25- and RIG-I-mediated antiviral innate immune signaling. In the other hand, nuclear lncRNA-*AVAN* positively regulates the transcription of forkhead box O3A (FOXO3a) *in cis* by associating with its promoter and inducing chromatin remodeling to enhance neutrophil chemotaxis.

FOXO3a is a member of the Forkhead box O (FoxO) family of transcription factors, which is a PTEN/PI3K/AKT effector functioning in diverse cellular activities such as the induction of cell-cycle arrest, stress resistance, apoptosis, differentiation, and metabolism (55-57). FOXO3a reportedly functions as a major transcriptional regulator in the maintenance of neutrophil activation during inflammation (58). However, little is known about the function of FOXO3a during the immune response in epithelial cells. Previous research demonstrated that FOXO3a repressed cytokine expression induced by LPS or bacteria (46). In this study, FOXO3a plays a different function during IAV infection. FOXO3a promotes IL-8 expression in IAV-infected A549 cells, which additionally enhances neutrophil chemotaxis. *AVAN* is located 1449-bp upstream of FOXO3a. We found that lncRNA-*AVAN* can markedly increase FOXO3a expression through chromatin remodeling in A549 cells. Additionally, *AVAN* can enhance neutrophil chemotaxis by upregulating the expression of IL-8. However, knockdown FOXO3a blocked the upregulation of IL-8 by *AVAN*. In the other hand, to confirm how much of the rise in the level of FOXO3a after AVAN overexpression is the result of enhanced IFN response, as opposed to a direct impact by AVAN on FOXO3a locus, we also used HL60 cells to evade IFN effects (data not shown here). Meanwhile, as seen in Figure 5, our data showed that there is a direct effect of AVAN on FOXO3a promoter and thereby enhanced Pol II

343 binding and H3K4me3 and H3K27ac accumulation. Of course, we would generate a mutant
344 AVAN that can induce IFN response similar to WT AVAN but can't bind the FOXO3a
345 promoter or change its expression level in subsequently studies. In addition, our results
346 exhibited that neutrophils were isolated from fresh peripheral blood and were infected in vitro
347 with influenza virus does not mimic their actual status in vivo. How and where AVAN is
348 induced in neutrophils need to be further investigated. Thus, we propose that *AVAN* may
349 enhance neutrophil chemotaxis through the regulation of FOXO3a expression. However, the
350 detailed mechanism by which FOXO3a regulates the expression of chemokines requires
351 further exploration.

352 Retinoic acid-inducible gene-I (RIG-I)-like receptors (RLRs) play a well-known role in
353 RNA virus recognition (59). Previous reports have shown that RIG-I is the main host sensor
354 involved in recognizing cytoplasmic viral RNA and subsequently initiating immune responses
355 to eliminate infection. TRIM25, an E3 ubiquitin ligase, is critically important in the RIG-I
356 signaling pathway. TRIM25 interacts with the CARD1 region of RIG-I and enhances RIG-I
357 polyubiquitylation to initiate RIG-I-mediated antivirus responses (47). A previous study found
358 that viruses have evolved sophisticated mechanisms to evade the host immune response
359 through regulating the role of TRIM25. IAV nonstructural protein 1 (NS1) specifically
360 inhibits TRIM25-mediated RIG-I CARD ubiquitination, thereby suppressing the RIG-I
361 signaling pathway (60). Our results demonstrated that the host can also regulate TRIM25 to
362 increase the immune response. *AVAN* can directly bind with the B box/central CCD of
363 TRIM25 in A549 cells. Furthermore, the interaction of *AVAN* with TRIM25 promotes the
364 association between TRIM25 and RIG-I and enhances RIG-I ubiquitylation, thereby

promoting IFN expression. It is worth noting that *AVAN* binds TRIM25 and facilitates IFN expression in mice. In addition, we explored the impact of AVAN overexpression or knockdown in IFN induction, chemo attraction of neutrophils or expression of cytokines and chemokines (Fig 3), speculated that lncRNA AVAN is critical in the IFN induction pathway. To the best of our knowledge, our work represents the first identification of lncRNA-*AVAN* as a novel partner of TRIM25 and demonstrates that *AVAN* suppresses IAV replication via TRIM25-RIG-I-dependent antiviral pathways.

In conclusion, we provide the first lncRNA landscape of IAV-infected patient neutrophils and identify the function of *AVAN*, a novel lncRNA, in the innate antiviral immune response. *AVAN* can enhance the chemotaxis of neutrophils by promoting FOXO3a expression *in cis.* On the one hand, *AVAN* can serve as a positive regulator of RIG-I signaling by directly binding TRIM25 and enhancing the association between TRIM25 and RIG-I *in trans*. (Fig 8). Of course, the mechanism of action of *AVAN in vivo* (transgenic mice) during IAV and its role in infection by other viruses warrant future investigations. Understanding the powerful roles of ubiquitous and versatile lncRNAs and identifying these IAV-related lncRNAs, especially the novel lncRNA-*AVAN*, may provide insights into the pathogenesis of viral infection, with lncRNA-*AVAN* potentially representing an essential target for intervention.

Materials and methods

Cells and viruses

A549 cells were cultured in DMEM/F12 (1:1) supplemented with 10% (v/v) FBS and penicillin-streptomycin (100 U/ml); 293T cells were cultured in DMEM/High Glucose supplemented with 10% (v/v) FBS and penicillin-streptomycin (100 U/ml); and HL60 and THP-1 cells were cultured in 1640 supplemented with 10% (v/v) FBS and penicillin-streptomycin (100 U/ml). The influenza virus A/Beijing/501/2009 (abbreviated as BJ501) and SeV used in this study were propagated by inoculation into 9 to 11-day-old specific pathogen-free (SPF) embryonated chicken eggs via the allantoic route as described previously. Virus stocks were aliquoted and stored at -80°C until use.

Mice

Pathogen-free 4-6-week-old female C57BL/6 mice were purchased from the Laboratory Animal Center, AMMS, Beijing, China. All procedures, including animal studies, were conducted following the National Guidelines for the Care of Laboratory Animals (2006-398) and performed in accordance with institutional regulations after protocol review and approval by the Institutional Animal Care and Use Committee of the Academy of Military Medical Sciences (project no. 2012-005). Mice were lightly anesthetized and subjected to i.n. inoculation with a tissue culture infective dose (TCID) of 10^5 TCID50 of BJ501 influenza virus in a volume of 20 μl per mouse. Control mice were inoculated with 20 μl of allantonic fluid. Inoculated mice were maintained under SPF conditions and monitored daily for weight loss and mortality or infection for 14 days post-infection. Survival rate, body weight changes,

405 histological examination and acute lung edema (wet-to-dry ratio) were determined as
406 described previously (61,62). The number of infiltrating inflammatory cells was counted and
407 presented as the number of cell per 200× field.

408

409 **RNA interference**

410 A549 and HL60 cells were transfected with siRNA targeting *AVAN*, FOXO3a, TRIM25 and
411 RIG-I using jetPRIME (Polyplus) according to the manufacturer's instructions. Two shRNA
412 were also used to knockdown *AVAN* in A549 cells. The siRNA and shRNA sequences used in
413 the experiments are listed in Supplementary Table S12.

414

415 **Neutrophils and monocyte isolation**

416 Neutrophils and monocyte were isolated from fresh peripheral blood using Percoll PLUS (GE
417 healthcare) according to the instructions supplied by the manufacturer. For neutrophils
418 collection, briefly, fresh peripheral blood was taken from IAV patients and healthy human
419 donors and layered on a 2-step Percoll PLUS gradient (75% and 60%), then centrifuged at
420 500×*g* for 25 minutes. The cells at the interface between 75% and 60% were collected and
421 washed twice with PBS and re-suspended in RPMI-1640 medium (Gibco) supplemented with
422 10% FBS and 100 U/ml penicillin-streptomycin at 37°C in a humidified atmosphere of 5%
423 (v/v) CO_2.

424

425 **ELISA**

426 Cytokines levels were measured using an ELISA kit (Dakewe, Beijing).

427

428 **Neutrophil chemotaxis assay**

429 *In vitro* chemotactic assays were performed in 24-well Millicell hanging-cell culture inserts
430 (Millipore). Briefly, the cells were starved by incubation for 18-24 h prior to the assay in
431 serum-free RPMI 1640 medium and then washed twice with sterile serum-free medium
432 containing 0.5% BSA. The bottom wells were loaded with the supernatant from
433 *AVAN*-overexpressing or knockdown A549 cells 24 h after BJ501 or PBS treatment to a final
434 volume of 300 μl. The top wells were loaded with neutrophils (10^6cells/ml; 250 μl from RPMI
435 suspension). The top and bottom wells were separated by a porous membrane (3-μm pore
436 size). A cover plate was added, and the cells were incubated for 1 h at 37°C with 5% CO_2. At
437 the end of the incubation period, the top wells were removed, and the number of cells in the
438 bottom wells was counted using a cell counter. The results are expressed as relative neutrophil
439 migration (number of cells from the tested group/number of cells from the corresponding
440 control vehicles).

441

442 **Antibodies and reagents**

443 The primary antibodies anti-RIG-I(D14G6), anti-TBK1(D1B4), anti-phospho-TBK1 (Ser172,
444 D52C2), anti-IRF3(D6I4C), anti-phospho-IRF3 (Ser396,4D4G), anti-β-Actin(13E5),
445 anti-FOXO3a, anti-H3K4me3 and anti-rabbit IgG, were purchased from Cell Signaling
446 Technology. Anti-Flag, anti-HA, anti-H3K27ac and anti-TRIM25 were purchased from Sigma.
447 Anti-Pol II was purchased from Abcam. Streptavidin C1 Beads were purchased from
448 Invitrogen. Protein A/G PLUS-Agarose were purchased from Santa Cruz. Protein A/G Beads

were purchased from Thermo Scientific. The western chemiluminescent HRP substrate was purchased from Millipore Corporation.

Western blotting

All cells were lysed in RIPA (Solarbio) supplemented with protease and phosphatase inhibitor cocktail (100×, Thermo Fisher) and lysed for 10 min on ice. The supernatant was mixed with 1/4 volume of 5× loading dye. The mixtures were then heated at 95°C and stored at –80°C. The samples were separated by SDS-PAGE and transferred onto nitrocellulose membranes. The membranes were then blocked with 5% nonfat milk (BD) in 1× Tris-buffered saline and 0.1% Triton 100 for 1 h while shaking at room temperature. Next, the membranes were incubated with primary antibodies and horseradish peroxidase–conjugated secondary antibodies. Bands were visualized using the Kodak film exposure detection system. The film was scanned, and the band intensity was analyzed using Quantity One software.

Quantitative real-time PCR

Total RNA was extracted from cultured cells using TRIzol reagent (Invitrogen). cDNA was generated by reverse transcription with commercial PrimeScript RT Master Mix (Takara). Primer pairs (Table S12) were designed using Primer Premier Software 5.0 (Premier Biosoft International, Palo Alto, CA) and synthesized by Invitrogen. Quantitative real-time PCR was performed in triplicate wells of a 96-well reaction plate on an ABI 7500 PCR System (Applied Biosystems). GAPDH was used as the endogenous control. The $2^{-\Delta\Delta Ct}$ method was used to calculate expression relative to the internal control. The data were analyzed using ABI

7500 SDS software v.1.3.

Luciferase assays

For IFNB1 transcriptional activity assays, 100 ng of pGL3-IFNB1 luciferase plasmid was cotransfected with 20 ng of pRL-TK vector into the cells using jetPRIME Transfection reagent (Polyplus). At 24 h after transfection, the cells were harvested according to the manufacturer's protocol (Promega), and firefly and Renilla luciferase signals were measured using a dual luciferase reporter assay system (Promega) on a Promega GloMax 96 machine (Promega) according to the protocol provided by the manufacturer.

Northern blotting

For northern blotting, total RNA was isolated from A549 cells using TRIzol reagent. Probes (Custom LNA mRNA Detection) were designed and synthesized by Exiqon and were also used for FISH. Northern blotting was performed as described previously (45).

5' and 3' RACE

The 5' and 3' RACE analyses were performed using the SMARTer RACE 5'/3' Kit (Clontech) according to the manufacturer's instructions. The RACE PCR products were cloned into pMD-19Tvector (Takara) and sequenced.

RNA pull-down assays

RNA pull-downs were performed as described (45). *In vitro* biotin-labeled RNAs (lnc*AVAN*

and its antisense RNA) were transcribed with biotin RNA labeling mix (Roche) and T7 RNA polymerase (Roche), treated with RNase-free DNase I (Promega) and purified using the RNeasy Mini Kit (QIAGEN). Biotinylated RNA was incubated with cell lysate, and precipitated proteins were separated via SDS-PAGE and subjected to MS.

RNA fluorescence *in situ* hybridization (RNA-FISH)

RNA-FISH was performed as described previously(48). Hybridization was carried out using DNA probe sets (Biosearch Technologies) according to the protocol provided by Biosearch Technologies. Cells were observed on a FV1000 confocal laser microscope (Olympus).

RNA immunoprecipitation (RIP) and chromatin immunoprecipitation (ChIP) assays

RIP assays were performed as described (48) with minor modification. Briefly, after incubation, the magnetic beads were washed with high salt lysis buffer (containing 500mM NaCl) 5 times. RIP products were analyzed by qRT-PCR using the primer pairs listed in Table S12**.** ChIP was performed as described (63). The ChIP-enriched FOXO3a promoter was quantified by qPCR using the primer pairs listed in Table S12.

ChIRP

ChIRP was performed according to Chu *et al* (64). Briefly, seven non-overlapping antisense DNA probes targeting *AVAN* were designed (http://www.singlemoleculefish.com), and eight probes targeting LacZ were also designed as non-specific controls. All probes were biotinylated at the 3’ end with an 18-carbon spacer arm (Invitrogen). 20 million cells were

cross-linked by 1% formaldehyde. Cross-linked cells were lysed in lysis buffer (50 mM Tris pH 7.0, 10 mM EDTA, 1% SDS, add DTT, PMSF, protease inhibitor, and RNase inhibitor before use) at 100mg/ml on ice for 10 min, and sonicated using Ultrasonic Cell Crusher on ice until the bulk of DNA smear is 100-500bp. The cell lysate was separated into two equal aliquots, one for hybridizing with probes targeting *AVAN*, and the other for probes targeting LacZ as control. Next, C-1 magnetic beads were added to the probe-chromatin mixture. After five total washes with washing buffer (2×SSC, 0.5% SDS, add DTT and PMSF before use), the beads were separated into two parts, 1/10 for RNA elution and 9/10 for DNA elution or protein elution. For elution of the RNA, the beads were treated with Protease K Buffer and RNA was extracted with Trizol reagent. For elution of the DNA, beads were treated with DNA Elution Buffer (50mM $NaHCO_3$, 1% SDS, add 100ug/ml RNase A and 100U/ml RNase H before use), and then DNA was isolated via phenol:chloroform:isoamyl alcohol extraction and subjected to qPCR. For elution of the protein, beads were treated with β-mercaptoethanol at a final concentration of 2.5% in 1× NuPAGE LDS Sample Buffer (Life Technologies, NP0007) at 96 °C for 30 min.

Statistical analyses

All data are presented as the means ± SEM. Data were analyzed using Student's t test. Survival data were analyzed by Kaplan-Meier survival analysis, and single time-points were analyzed using ANOVA. All analyses are performed using Instat software (Version 5.0, GraphPad prism). $p<0.05$ was considered statistically significant.

Acknowledgments

This work was supported in part by funding from the National Programs for High Technology Research and Development of China (SS2015AA020924) , the National Major Research and Development Program of China (No. 2017YFC1200800) and the Natural Science Foundation of China (81771700).

Author contributions

Authors P.Y., R.C. and X.W. conceived and designed the experiments; C.L., L.L., Q.L., S.C., K.W., L.Z., M.X. and H.G. performed the experiments; Y.D., C.W., Z.Z., L.Z., J. S., Z. L. and J.L. analyzed the data; and C.L., L.L., K.W. and Q.L. wrote the manuscript.

Competing interests

None of the authors have competing financial interests to declare.

552 **Fig legends**

553 **Fig 1 LncRNA expression is regulated by the influenza A virus**

554 (A) Gene ontology (GO) analysis of differentially expressed genes in IAV-infected patient
555 neutrophils compared with their recovery-stage counterparts from RNA-seq data (FC>2;
556 p<0.05). The top six most significantly enriched GO terms are shown.

557 (B) Cluster heat map showing differentially expressed lncRNAs in IAV-infected patient
558 neutrophils compared with recovery-stage samples based on RNA-seq data (FC>2; p <0.05).

559 (C) Cluster heat map showing 26 lncRNA candidates selected via *in silico* analysis from the
560 RNA-seq data (FC>2; p <0.05).

561 (D-E) The expression of 26 lncRNA candidates in neutrophils (D) and monocyte (E) from
562 healthy volunteers stimulated with BJ501 (MOI=0.5) or mock for 12 h by qRT-PCR analysis
563 (n=3; means ± SEM; *p<0.05;**p<0.01;***p<0.001).

564 (F) The expression of 26 lncRNA candidates in A549 cells stimulated with BJ501 (MOI=1) or
565 mock for 24 h by qRT-PCR analysis (n=3; means ± SEM; *p<0.05; **p<0.01; ***p<0.001).

566

567 **Fig 2 *AVAN* is highly expressed in viral infection**

568 (A) *AVAN* expression in IAV-infected patient neutrophils by qRT-PCR analysis (healthy
569 controls=18; patients=63; *p<0.05).

570 (B) *AVAN* expression in A549 cells infected with BJ501 (MOI=1), H5N1 (MOI=1), H7N9
571 (MOI=1), PR8 (MOI=1), H3N2 (MOI=1), Sendai virus (SeV) (MOI=1), or respiratory
572 syncytial virus (RSV) (MOI=1) for 24 h by qRT-PCR analysis.

573 (C and D) *AVAN* expression in A549 cells infected with BJ501 at an MOI of 1 for the

574 indicated times (C) or at the indicated MOIs for 24 h (D) by qRT-PCR analysis.

575 (E) Fractionation of BJ501-infected A549 cells followed by qRT-PCR analysis. The U1 and
576 U6 RNAs served as positive controls for nuclear gene expression. The ACTIN and GAPDH
577 RNAs served as positive controls for cytoplasmic gene expression. N, nuclear fraction; C,
578 cytoplasmic fraction.

579 (F) AVAN intracellular localization visualized by RNA-FISH in A549 cells stimulated with
580 MOCK (left) or BJ501 (MOI=1) (right) for 24 h. DAPI, 4',6-diamidino-2-phenylindole.
581 Probe 1 and 2, AVAN. Scale bar, 10 μm.

582 (G) Northern blotting of *AVAN* in A549 cells treated with mock or BJ501 (MOI=1) at 24h
583 post-infection.

584

585 **Fig 3 Altered *AVAN* expression has profound effects on type I interferon and neutrophil**
586 **chemotaxis.**

587 (A) The efficiency of *AVAN* overexpression was determined by qRT-PCR in BJ501-infected
588 A549 cells.

589 (B and I) BJ501 replication in *AVAN*-overexpressing (B) and *AVAN*-knockdown (I) A549 cells
590 examined by the $TCID_{50}$ assay (MOI=1). The virus titers in supernatants were measured at 24
591 h post-infection.

592 (C, D, J and K) IFN-α and IFN-β expression in A549 cells measured by qRT-PCR and ELISA
593 (MOI=1) at 24 h post-infection.

594 (E and L) Transwell assay of neutrophil migration in *AVAN*-overexpressing or
595 *AVAN*-knockdown A549 culture supernatants.

596 (F and M) IL-8 expression in A549 cells were measured by qRT-PCR (MOI=1) at 24 h
597 post-infection.
598 (G and N) IL-8 expression in A549 cells were measured by ELISA (MOI=1) at 24 h
599 post-infection.
600 (H) The efficiency of AVAN knockdown was determined by qRT-PCR in BJ501-uninfected or
601 -infected A549 cells.
602
603 **Fig 4 *AVAN* up-regulates ISG and chemokine expression**
604 (A) Cluster heat map showing altered mRNA expression in *AVAN*-overexpressing A549 cells
605 and EV control A549 cells infected with BJ501 (MOI=1) for 14 h by cDNA microarray (n=3;
606 FC>1.3; $p<0.05$).
607 (B) Reactome pathway analysis of the altered mRNA expression from the cDNA microarray
608 analysis.
609 (C) Cluster heat map showing the altered expression of mRNAs involved with ISGs and
610 cytokine mRNAs that were up-regulated during *AVAN* overexpression.
611 (D) The mRNA levels of selected genes in *AVAN*-overexpressing A549 cells and EV control
612 A549 cells infected with BJ501 (MOI=1) for 14 h by qRT-PCR analysis.
613
614 **Fig 5 *AVAN* enhances FOXO3a expression *in cis***
615 (A and B) FOXO3a expression during virus infection in A549 cells were measured by
616 qRT-PCR. A549 cells were transfected with *AVAN* plasmids (A) or siRNA (B).
617 (C) Enrichement of AVAN in ChIRP assay analyzed by qRT-PCR, U1 as a negative control.

(D and E) ChIRP assay showing that AVAN binds directly to the FOXO3a promoter and DNA in BJ501-uninfected (D) and -infected (E) A549 cells.

(F-K) H3K4me3 and H3K27ac levels and Pol II binding of the FOXO3a promoter were analyzed through ChIP followed byqRT-PCR in BJ501-infected A549 cells.

(L and M) Transwell assay of neutrophil migration in FOXO3a-overexpressing or FOXO3a-knockdown A549 culture supernatant.

(N and O) IL-8 expression in FOXO3a-overexpressing (N) or FOXO3a-knockdown (O)A549 cells were measured by qRT-PCR.

(O) IL-8 expression in *AVAN*-overexpressing or/and FOXO3a-knockdown A549 cells were measured by qRT-PCR.

Fig 6 *AVAN* direct binds to TRIM25 and enhances the antivirus immune response

(A) RNA pull-down of *AVAN*-associated proteins using biotinylated AVAN or antisense probes. Isolated proteins were resolved by SDS-PAGE followed by silver staining.

(B) Pull-down western blot showing that *AVAN* can bind directly to TRIM25.

(C) ChIRP followed by western blot show that *AVAN* can bind to TRIM25.

(D and E) Exogenous (D) and endogenous (E) RIP of TRIM25 in BJ501 infected cells using anti-TRIM25 or anti-IgG antibodies. The relative enrichment fold of *AVAN* was calculated by qRT-PCR.

(F) *AVAN* pull-down western blot with lysates of A549 cells transfected with Flag, Flag-TRIM25, Flag-SPRY, Flag-B Box/CCD or Flag-Ring.

(G) Truncated *AVAN* pull-down, truncates (upper panel) were obtained via *in vitro*

640 transcription and incubated with BJ501-infected A549 lysates for RNA pulldown.

641 (H) TRIM25 co-immunoprecipitation with proteins from lysates of BJ501-infected A549 cells
642 transfected with *AVAN*s, followed by immunoblotting. Anti-TRIM25 and anti-RIG-I
643 antibodies were used for immunoprecipitated.

644 (I) Immunoblot analysis of endogenous RIG-I ubiquitylation in control and
645 *AVAN*-overexpressing A549 cells transfected with BJ501. Anti-RIG-I antibody was used for
646 immunoprecipitated.

647 (J) Immunoblot analysis of proteins immunoprecipitated with anti-Flag from lysates of A549
648 cells transfected with *AVAN*, HA-Ub and Flag-tagged RIG-I.

649 (K) Western blot analysis of RIG-I signaling in A549 cells transfected with *AVAN* or siRNAs.
650 *AVAN* enhances RIG-I signaling activation.

651 (L and M) IFN-alpha (L) and IFN-beta (M) expression upon AVAN transfection in A549 cells
652 that were infected by BJ501 or not (MOI=1) at 24h post-infection, and then individually
653 knock down RIG-I or TRIM25, analyzed by qRT_PCR.

654

655 **Fig 7 *AVAN* protects mice from virus infection**

656 (A) *AVAN* expression in the lung of AAV2/9-*AVAN*-treated or control mice measured by
657 RT-PCR.

658 (B and C) Four-week-old wild-type B6 mice were inoculated with $10^{5.125}$ $TCID_{50}$ BJ501 virus.
659 Survival rates (B) and body weight changes (C) of wild-type mice (n=10 for each group) were
660 monitored for 2 weeks after BJ501 challenge.

661 (D) Wet:dry ratios of lung tissues (n=6 for each group) at 5 DPI.

(E and F) HE-stained images (E) and infiltrating cell counts (F) (n=100 fields) in lung tissues at 5 DPI (magnification=200×). *p<0.05, **p<0.01 and ***p<0.001.

(G and H) Lung HA titer (G) and virus titer (H) at 5 DPI (magnification=200×). *p<0.05, **p<0.01.

(I) Immunoblot analysis showing that *AVAN* can bind to Trim25 *in vivo*.

(J) IFN-α and IFN-β expression in the lung of mice treated with AAV2/9-*AVAN* or control vector measured by qRT-PCR

Fig 8 Schematic of the mechanisms by which *AVAN* regulates antivirus responses and neutrophil chemotaxis.

References

1. Fatica, A. and Bozzoni, I. (2014) Long non-coding RNAs: new players in cell differentiation and development. *Nature reviews. Genetics*, **15**, 7-21.
2. Batista, P.J. and Chang, H.Y. (2013) Long noncoding RNAs: cellular address codes in development and disease. *Cell*, **152**, 1298-1307.
3. Devaux, Y., Zangrando, J., Schroen, B., Creemers, E.E., Pedrazzini, T., Chang, C.P., Dorn, G.W., 2nd, Thum, T., Heymans, S. and Cardiolinc, n. (2015) Long noncoding RNAs in cardiac development and ageing. *Nature reviews. Cardiology*, **12**, 415-425.
4. Chen, C.K., Blanco, M., Jackson, C., Aznauryan, E., Ollikainen, N., Surka, C., Chow, A., Cerase, A., McDonel, P. and Guttman, M. (2016) Xist recruits the X chromosome to the nuclear lamina to enable chromosome-wide silencing. *Science*, **354**, 468-472.
5. McHugh, C.A., Chen, C.K., Chow, A., Surka, C.F., Tran, C., McDonel, P., Pandya-Jones, A., Blanco, M., Burghard, C., Moradian, A. *et al.* (2015) The Xist lncRNA interacts directly with SHARP to silence transcription through HDAC3. *Nature*, **521**, 232-236.
6. Patil, D.P., Chen, C.K., Pickering, B.F., Chow, A., Jackson, C., Guttman, M. and Jaffrey, S.R. (2016) m(6)A RNA methylation promotes XIST-mediated transcriptional repression. *Nature*, **537**, 369-373.
7. Schmitt, A.M. and Chang, H.Y. (2016) Long Noncoding RNAs in Cancer Pathways. *Cancer cell*, **29**, 452-463.
8. Lee, J.T. and Bartolomei, M.S. (2013) X-inactivation, imprinting, and long noncoding RNAs in health and disease. *Cell*, **152**, 1308-1323.
9. Xu, C., Zhang, Y., Wang, Q., Xu, Z., Jiang, J., Gao, Y., Gao, M., Kang, J., Wu, M., Xiong, J. *et al.* (2016) Long non-coding RNA GAS5 controls human embryonic stem cell self-renewal by maintaining NODAL signalling. *Nature communications*, **7**, 13287.
10. Zhou, J., Wang, D., Gao, R., Zhao, B., Song, J., Qi, X., Zhang, Y., Shi, Y., Yang, L., Zhu, W. *et al.* (2013) Biological features of novel avian influenza A (H7N9) virus. *Nature*, **499**, 500-503.
11. Satpathy, A.T. and Chang, H.Y. (2015) Long noncoding RNA in hematopoiesis and immunity. *Immunity*, **42**, 792-804.
12. Fitzgerald, K.A. and Caffrey, D.R. (2014) Long noncoding RNAs in innate and adaptive immunity. *Current opinion in immunology*, **26**, 140-146.
13. Carpenter, S., Aiello, D., Atianand, M.K., Ricci, E.P., Gandhi, P., Hall, L.L., Byron, M., Monks, B., Henry-Bezy, M., Lawrence, J.B. *et al.* (2013) A long noncoding RNA mediates both activation and repression of immune response genes. *Science*, **341**, 789-792.
14. Chen, Y.G., Satpathy, A.T. and Chang, H.Y. (2017) Gene regulation in the immune system by long noncoding RNAs. *Nature immunology*, **18**, 962-972.
15. Holoch, D. and Moazed, D. (2015) RNA-mediated epigenetic regulation of gene expression. *Nature reviews. Genetics*, **16**, 71-84.
16. Yuan, J.H., Liu, X.N., Wang, T.T., Pan, W., Tao, Q.F., Zhou, W.P., Wang, F. and Sun, S.H. (2017) The MBNL3 splicing factor promotes hepatocellular carcinoma by increasing PXN expression through the alternative splicing of lncRNA-PXN-AS1. *Nature cell biology*, **19**, 820-832.
17. Pefanis, E., Wang, J., Rothschild, G., Lim, J., Kazadi, D., Sun, J., Federation, A., Chao, J., Elliott, O., Liu, Z.P. *et al.* (2015) RNA exosome-regulated long non-coding RNA transcription controls super-enhancer activity. *Cell*, **161**, 774-789.
18. Mercer, T.R. and Mattick, J.S. (2013) Structure and function of long noncoding RNAs in epigenetic regulation. *Nature structural & molecular biology*, **20**, 300-307.

19. Jiang, M., Zhang, S., Yang, Z., Lin, H., Zhu, J., Liu, L., Wang, W., Liu, S., Liu, W., Ma, Y. *et al.* (2018) Self-Recognition of an Inducible Host lncRNA by RIG-I Feedback Restricts Innate Immune Response. *Cell*, **173**, 906-919 e913.
20. Everitt, A.R., Clare, S., Pertel, T., John, S.P., Wash, R.S., Smith, S.E., Chin, C.R., Feeley, E.M., Sims, J.S., Adams, D.J. *et al.* (2012) IFITM3 restricts the morbidity and mortality associated with influenza. *Nature*, **484**, 519-523.
21. Futosi, K., Fodor, S. and Mocsai, A. (2013) Reprint of Neutrophil cell surface receptors and their intracellular signal transduction pathways. *International immunopharmacology*, **17**, 1185-1197.
22. Tecchio, C., Micheletti, A. and Cassatella, M.A. (2014) Neutrophil-derived cytokines: facts beyond expression. *Frontiers in immunology*, **5**, 508.
23. Wang, K., Lai, C., Li, T., Wang, C., Wang, W., Ni, B., Bai, C., Zhang, S., Han, L., Gu, H. *et al.* (2017) Basic fibroblast growth factor protects against influenza A virus-induced acute lung injury by recruiting neutrophils. *Journal of molecular cell biology*.
24. Tumpey, T.M., Garcia-Sastre, A., Taubenberger, J.K., Palese, P., Swayne, D.E., Pantin-Jackwood, M.J., Schultz-Cherry, S., Solorzano, A., Van Rooijen, N., Katz, J.M. *et al.* (2005) Pathogenicity of influenza viruses with genes from the 1918 pandemic virus: functional roles of alveolar macrophages and neutrophils in limiting virus replication and mortality in mice. *Journal of virology*, **79**, 14933-14944.
25. Perrone, L.A., Plowden, J.K., Garcia-Sastre, A., Katz, J.M. and Tumpey, T.M. (2008) H5N1 and 1918 pandemic influenza virus infection results in early and excessive infiltration of macrophages and neutrophils in the lungs of mice. *PLoS pathogens*, **4**, e1000115.
26. Baskin, C.R., Bielefeldt-Ohmann, H., Garcia-Sastre, A., Tumpey, T.M., Van Hoeven, N., Carter, V.S., Thomas, M.J., Proll, S., Solorzano, A., Billharz, R. *et al.* (2007) Functional genomic and serological analysis of the protective immune response resulting from vaccination of macaques with an NS1-truncated influenza virus. *Journal of virology*, **81**, 11817-11827.
27. Cassatella, M.A. (1999) Neutrophil-derived proteins: selling cytokines by the pound. *Advances in immunology*, **73**, 369-509.
28. Sadik, C.D., Kim, N.D. and Luster, A.D. (2011) Neutrophils cascading their way to inflammation. *Trends in immunology*, **32**, 452-460.
29. Blander, J.M. (2014) A long-awaited merger of the pathways mediating host defence and programmed cell death. *Nature reviews. Immunology*, **14**, 601-618.
30. Kell, A.M. and Gale, M., Jr. (2015) RIG-I in RNA virus recognition. *Virology*, **479-480**, 110-121.
31. Kandasamy, M., Suryawanshi, A., Tundup, S., Perez, J.T., Schmolke, M., Manicassamy, S. and Manicassamy, B. (2016) RIG-I Signaling Is Critical for Efficient Polyfunctional T Cell Responses during Influenza Virus Infection. *PLoS pathogens*, **12**, e1005754.
32. Yuan, J.H., Yang, F., Wang, F., Ma, J.Z., Guo, Y.J., Tao, Q.F., Liu, F., Pan, W., Wang, T.T., Zhou, C.C. *et al.* (2014) A long noncoding RNA activated by TGF-beta promotes the invasion-metastasis cascade in hepatocellular carcinoma. *Cancer cell*, **25**, 666-681.
33. Deng, L., Yang, S.B., Xu, F.F. and Zhang, J.H. (2015) Long noncoding RNA CCAT1 promotes hepatocellular carcinoma progression by functioning as let-7 sponge. *Journal of experimental & clinical cancer research : CR*, **34**, 18.
34. Iwasaki, A. and Pillai, P.S. (2014) Innate immunity to influenza virus infection. *Nature reviews. Immunology*, **14**, 315-328.
35. Tavares, L.P., Teixeira, M.M. and Garcia, C.C. (2017) The inflammatory response triggered by Influenza virus: a two edged sword. *Inflammation research : official journal of the European Histamine Research Society ... [et al.]*, **66**, 283-302.

36. Durbin, R.K., Kotenko, S.V. and Durbin, J.E. (2013) Interferon induction and function at the mucosal surface. *Immunological reviews*, **255**, 25-39.
37. de Boer, W.I., Sont, J.K., van Schadewijk, A., Stolk, J., van Krieken, J.H. and Hiemstra, P.S. (2000) Monocyte chemoattractant protein 1, interleukin 8, and chronic airways inflammation in COPD. *The Journal of pathology*, **190**, 619-626.
38. Scapini, P., Lapinet-Vera, J.A., Gasperini, S., Calzetti, F., Bazzoni, F. and Cassatella, M.A. (2000) The neutrophil as a cellular source of chemokines. *Immunological reviews*, **177**, 195-203.
39. Qiu, L., Zhang, H., Yang, K. and Jiang, S. (2009) Molecular cloning and mRNA expression analysis of interleukin-8 gene in Japanese sea perch (Lateolabrax japonicus). *Molecular biology reports*, **36**, 1099-1105.
40. Chu, C.Q., Lu, X.J., Li, C.H. and Chen, J. (2014) Molecular characterization of a CXCL8-like protein from ayu and its effect on chemotaxis of neutrophils and monocytes/macrophages. *Gene*, **548**, 48-55.
41. Wang, K.C., Yang, Y.W., Liu, B., Sanyal, A., Corces-Zimmerman, R., Chen, Y., Lajoie, B.R., Protacio, A., Flynn, R.A., Gupta, R.A. *et al.* (2011) A long noncoding RNA maintains active chromatin to coordinate homeotic gene expression. *Nature*, **472**, 120-124.
42. Anderson, K.M., Anderson, D.M., McAnally, J.R., Shelton, J.M., Bassel-Duby, R. and Olson, E.N. (2016) Transcription of the non-coding RNA upperhand controls Hand2 expression and heart development. *Nature*, **539**, 433-436.
43. Engreitz, J.M., Haines, J.E., Perez, E.M., Munson, G., Chen, J., Kane, M., McDonel, P.E., Guttman, M. and Lander, E.S. (2016) Local regulation of gene expression by lncRNA promoters, transcription and splicing. *Nature*, **539**, 452-455.
44. Paralkar, V.R., Taborda, C.C., Huang, P., Yao, Y., Kossenkov, A.V., Prasad, R., Luan, J., Davies, J.O., Hughes, J.R., Hardison, R.C. *et al.* (2016) Unlinking an lncRNA from Its Associated cis Element. *Molecular cell*, **62**, 104-110.
45. Xiao, T., Liu, L., Li, H., Sun, Y., Luo, H., Li, T., Wang, S., Dalton, S., Zhao, R.C. and Chen, R. (2015) Long Noncoding RNA ADINR Regulates Adipogenesis by Transcriptionally Activating C/EBPalpha. *Stem cell reports*, **5**, 856-865.
46. Snoeks, L., Weber, C.R., Turner, J.R., Bhattacharyya, M., Wasland, K. and Savkovic, S.D. (2008) Tumor suppressor Foxo3a is involved in the regulation of lipopolysaccharide-induced interleukin-8 in intestinal HT-29 cells. *Infection and immunity*, **76**, 4677-4685.
47. Gack, M.U., Shin, Y.C., Joo, C.H., Urano, T., Liang, C., Sun, L., Takeuchi, O., Akira, S., Chen, Z., Inoue, S. *et al.* (2007) TRIM25 RING-finger E3 ubiquitin ligase is essential for RIG-I-mediated antiviral activity. *Nature*, **446**, 916-920.
48. Liu, L., Yue, H., Liu, Q., Yuan, J., Li, J., Wei, G., Chen, X., Lu, Y., Guo, M., Luo, J. *et al.* (2016) LncRNA MT1JP functions as a tumor suppressor by interacting with TIAR to modulate the p53 pathway. *Oncotarget*, **7**, 15787-15800.
49. Josset, L., Tchitchek, N., Gralinski, L.E., Ferris, M.T., Eisfeld, A.J., Green, R.R., Thomas, M.J., Tisoncik-Go, J., Schroth, G.P., Kawaoka, Y. *et al.* (2014) Annotation of long non-coding RNAs expressed in collaborative cross founder mice in response to respiratory virus infection reveals a new class of interferon-stimulated transcripts. *RNA biology*, **11**, 875-890.
50. Winterling, C., Koch, M., Koeppel, M., Garcia-Alcalde, F., Karlas, A. and Meyer, T.F. (2014) Evidence for a crucial role of a host non-coding RNA in influenza A virus replication. *RNA biology*, **11**, 66-75.
51. Yin, Z., Guan, D., Fan, Q., Su, J., Zheng, W., Ma, W. and Ke, C. (2013) lncRNA expression signatures in response to enterovirus 71 infection. *Biochemical and biophysical research communications*, **430**, 629-633.

52. Fortes, P. and Morris, K.V. (2016) Long noncoding RNAs in viral infections. *Virus research*, **212**, 1-11.
53. Ouyang, J., Zhu, X., Chen, Y., Wei, H., Chen, Q., Chi, X., Qi, B., Zhang, L., Zhao, Y., Gao, G.F. *et al.* (2014) NRAV, a long noncoding RNA, modulates antiviral responses through suppression of interferon-stimulated gene transcription. *Cell host & microbe*, **16**, 616-626.
54. Jiang M., Zhang S., Yang Z. , Lin H., Zhu J. , Liu L., Wang W., Liu S., Liu W., Ma Y. *et al.* (2018) Self-Recognition of an Inducible Host lncRNA by RIG-I Feedback Restricts Innate Immune Response. *Cell*, **173**, 1-14.
55. Brunet, A., Bonni, A., Zigmond, M.J., Lin, M.Z., Juo, P., Hu, L.S., Anderson, M.J., Arden, K.C., Blenis, J. and Greenberg, M.E. (1999) Akt promotes cell survival by phosphorylating and inhibiting a Forkhead transcription factor. *Cell*, **96**, 857-868.
56. Furukawa-Hibi, Y., Yoshida-Araki, K., Ohta, T., Ikeda, K. and Motoyama, N. (2002) FOXO forkhead transcription factors induce G(2)-M checkpoint in response to oxidative stress. *The Journal of biological chemistry*, **277**, 26729-26732.
57. Miyamoto, K., Miyamoto, T., Kato, R., Yoshimura, A., Motoyama, N. and Suda, T. (2008) FoxO3a regulates hematopoietic homeostasis through a negative feedback pathway in conditions of stress or aging. *Blood*, **112**, 4485-4493.
58. Jonsson, H., Allen, P. and Peng, S.L. (2005) Inflammatory arthritis requires Foxo3a to prevent Fas ligand-induced neutrophil apoptosis. *Nature medicine*, **11**, 666-671.
59. Zhao, C., Jia, M., Song, H., Yu, Z., Wang, W., Li, Q., Zhang, L., Zhao, W. and Cao, X. (2017) The E3 Ubiquitin Ligase TRIM40 Attenuates Antiviral Immune Responses by Targeting MDA5 and RIG-I. *Cell reports*, **21**, 1613-1623.
60. Gack, M.U., Albrecht, R.A., Urano, T., Inn, K.S., Huang, I.C., Carnero, E., Farzan, M., Inoue, S., Jung, J.U. and Garcia-Sastre, A. (2009) Influenza A virus NS1 targets the ubiquitin ligase TRIM25 to evade recognition by the host viral RNA sensor RIG-I. *Cell host & microbe*, **5**, 439-449.
61. Wang, W., Yang, P., Zhong, Y., Zhao, Z., Xing, L., Zhao, Y., Zou, Z., Zhang, Y., Li, C., Li, T. *et al.* (2013) Monoclonal antibody against CXCL-10/IP-10 ameliorates influenza A (H1N1) virus induced acute lung injury. *Cell research*, **23**, 577-580.
62. Li, C., Yang, P., Sun, Y., Li, T., Wang, C., Wang, Z., Zou, Z., Yan, Y., Wang, W., Wang, C. *et al.* (2012) IL-17 response mediates acute lung injury induced by the 2009 pandemic influenza A (H1N1) virus. *Cell research*, **22**, 528-538.
63. Nelson, J.D., Denisenko, O. and Bomsztyk, K. (2006) Protocol for the fast chromatin immunoprecipitation (ChIP) method. *Nature protocols*, **1**, 179-185.
64. Chu, C., Quinn, J. and Chang, H.Y. (2012) Chromatin isolation by RNA purification (ChIRP). *Journal of visualized experiments : JoVE*.

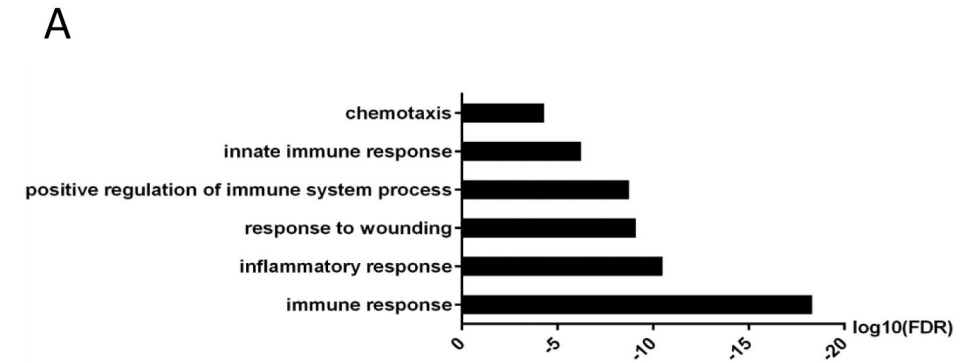

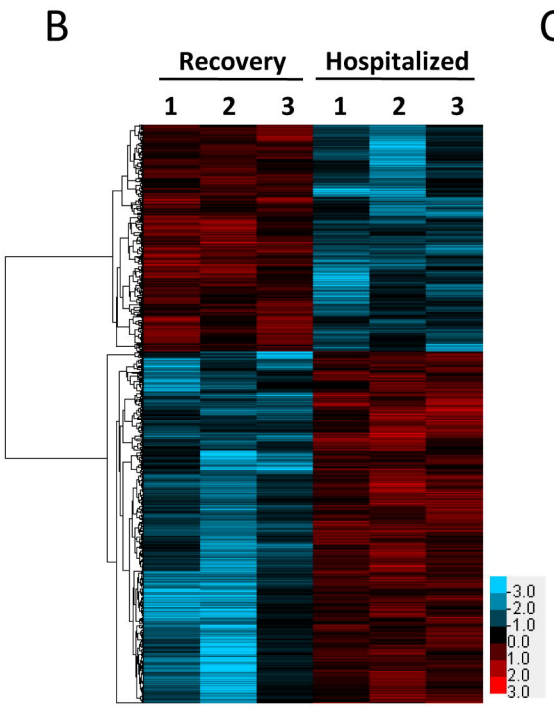

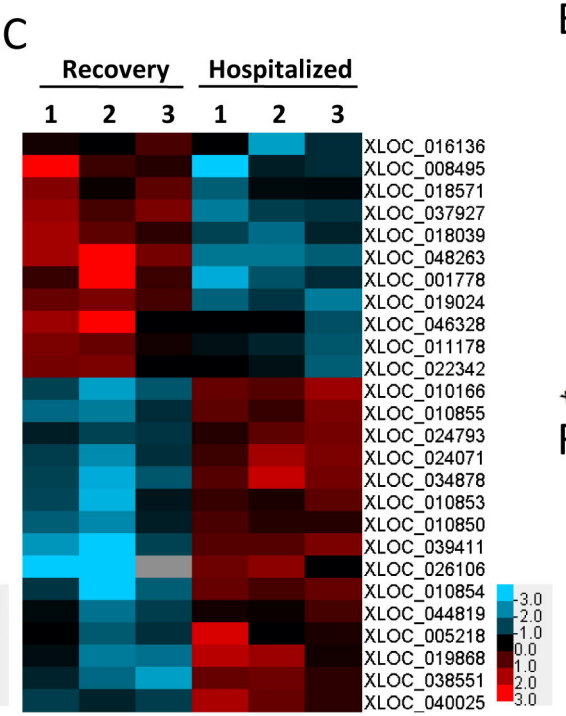

FC>2, p<0.05
Up-regulated: 240(164-357)
Down-regulated: 193(158-257)

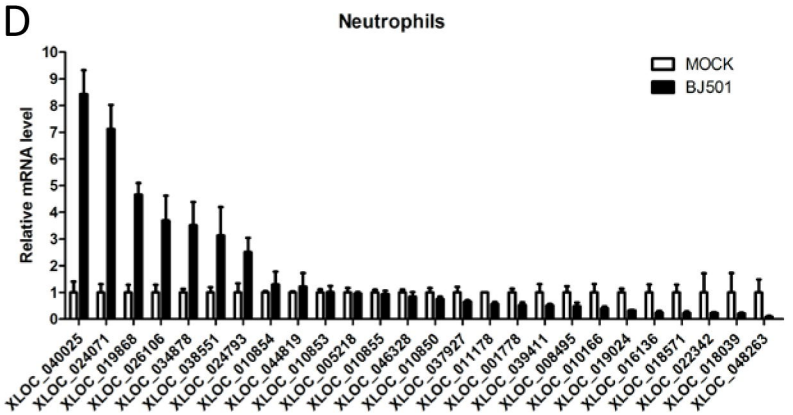

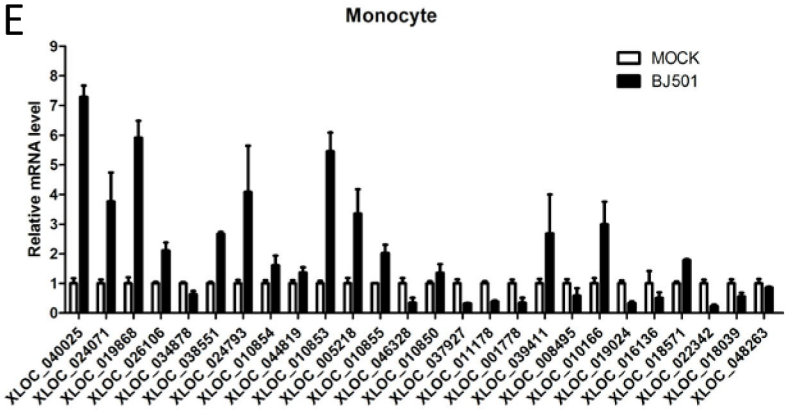

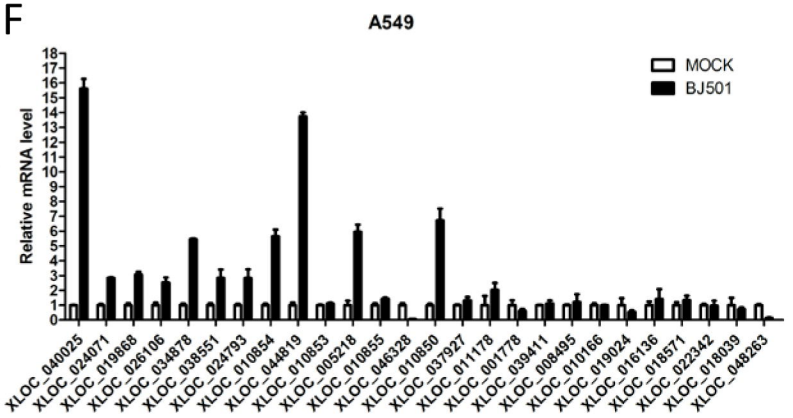

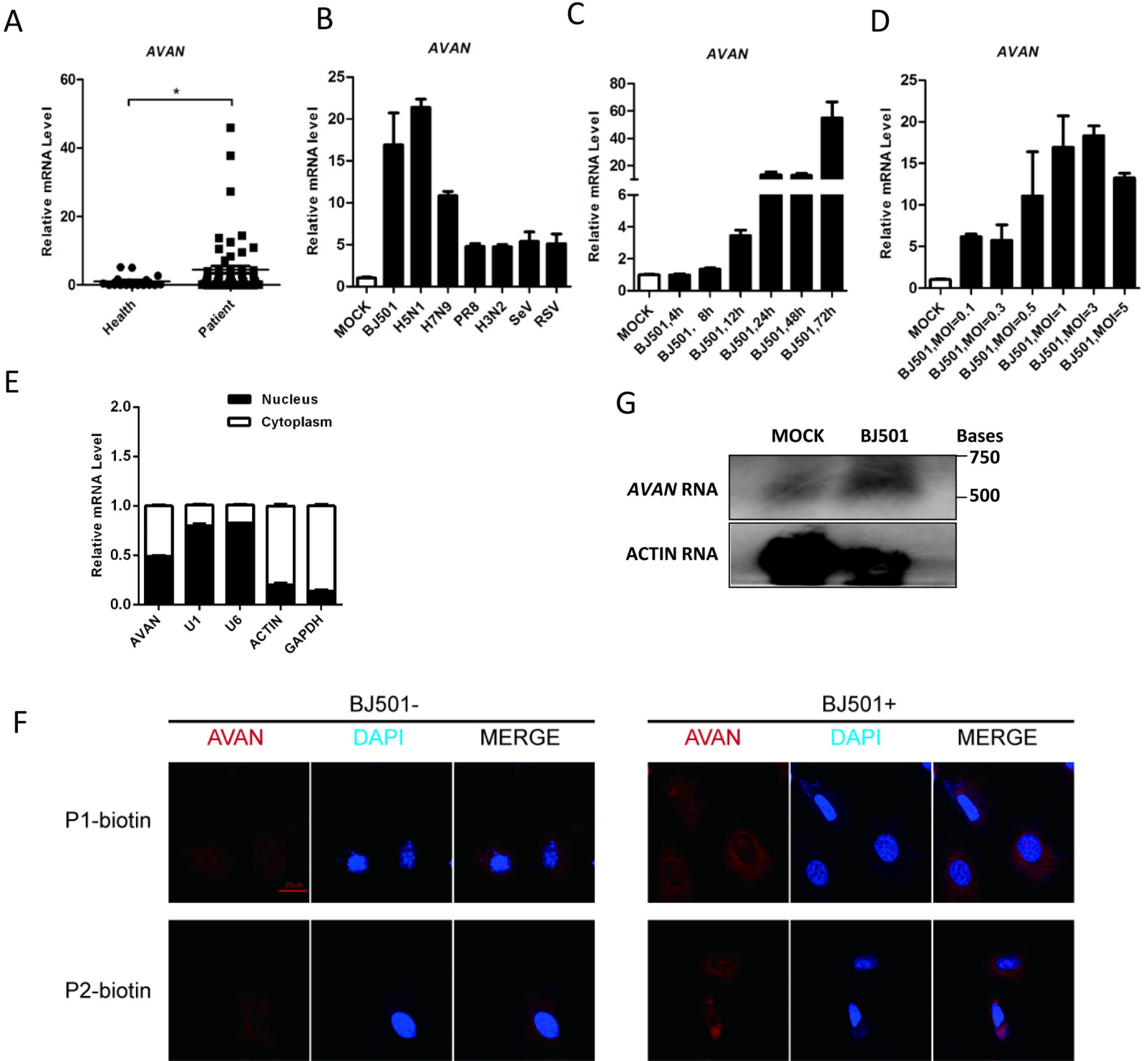
A
AVAN
Relative mRNA Level
60
40
20
0
*
Health
Patient
B
AVAN
Relative mRNA level
25
20
15
10
5
0
MOCK
BJ501
H5N1
H7N9
PR8
H3N2
SeV
RSV
C
AVAN
Relative mRNA Level
80
60
40
20
6
4
2
0
MOCK
BJ501,4h
BJ501, 8h
BJ501,12h
BJ501,24h
BJ501,48h
BJ501,72h
D
AVAN
Relative mRNA Level
25
20
15
10
5
0
MOCK
BJ501,MOI=0.1
BJ501,MOI=0.3
BJ501,MOI=0.5
BJ501,MOI=1
BJ501,MOI=3
BJ501,MOI=5
E
Nucleus
Cytoplasm
Relative mRNA Level
2.0
1.5
1.0
0.5
0.0
AVAN
U1
U6
ACTIN
GAPDH
G
MOCK
BJ501
Bases
750
500
AVAN RNA
ACTIN RNA
F
BJ501-
BJ501+
AVAN
DAPI
MERGE
AVAN
DAPI
MERGE
P1-biotin
P2-biotin

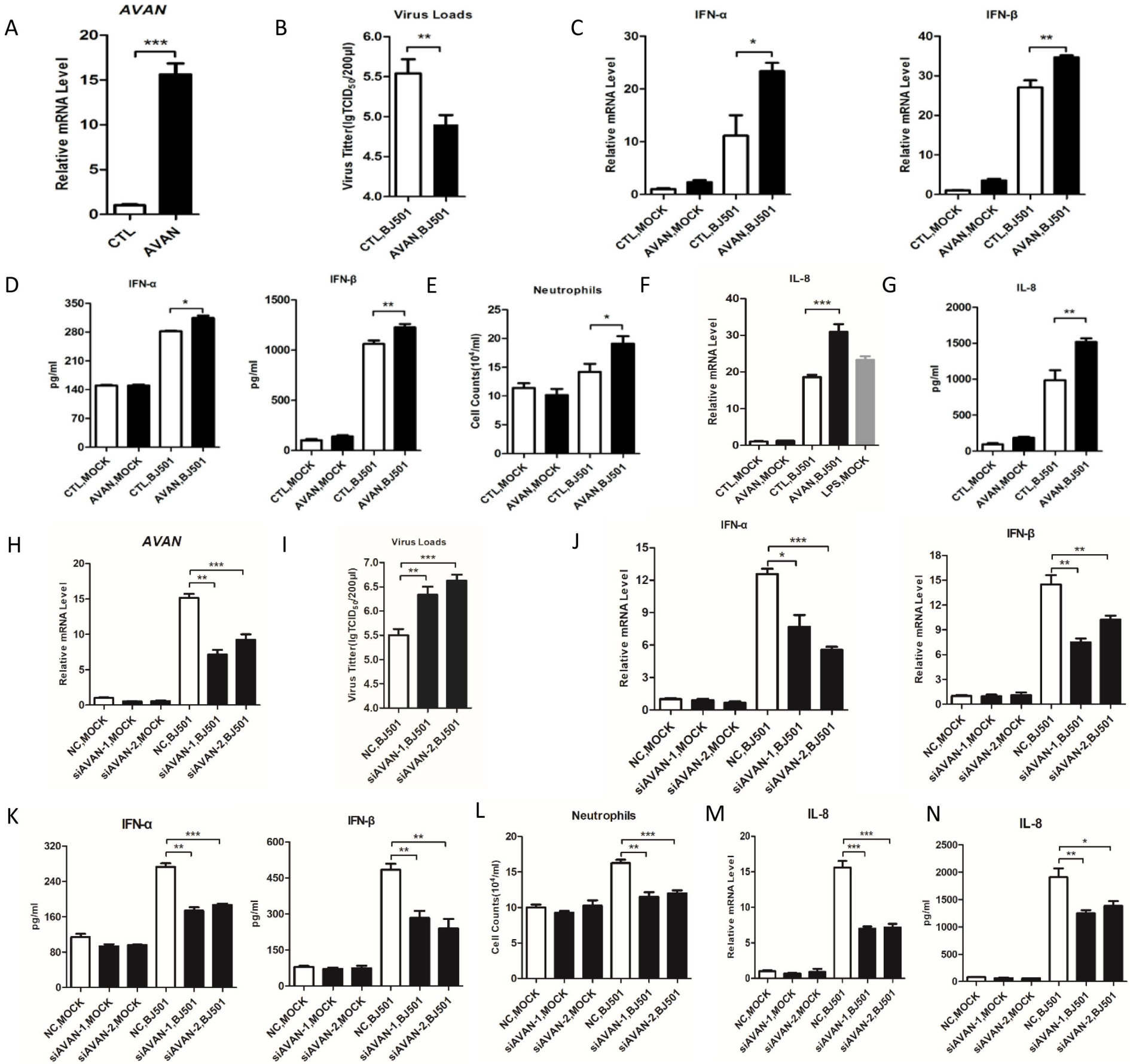
A
AVAN
Relative mRNA Level
CTL
AVAN
B
Virus Loads
Virus Titter(lgTCID50/200μl)
CTL,BJ501
AVAN,BJ501
C
IFN-α
IFN-β
Relative mRNA Level
CTL,MOCK
AVAN,MOCK
CTL,BJ501
AVAN,BJ501
D
IFN-α
IFN-β
pg/ml
E
Neutrophils
Cell Counts(10⁴/ml)
F
IL-8
Relative mRNA Level
LPS,MOCK
G
IL-8
pg/ml
H
AVAN
Relative mRNA Level
NC,MOCK
siAVAN-1,MOCK
siAVAN-2,MOCK
NC,BJ501
siAVAN-1,BJ501
siAVAN-2,BJ501
I
Virus Loads
Virus Titter(lgTCID50/200μl)
J
IFN-α
IFN-β
Relative mRNA Level
K
IFN-α
IFN-β
pg/ml
L
Neutrophils
Cell Counts(10⁴/ml)
M
IL-8
Relative mRNA Level
N
IL-8
pg/ml

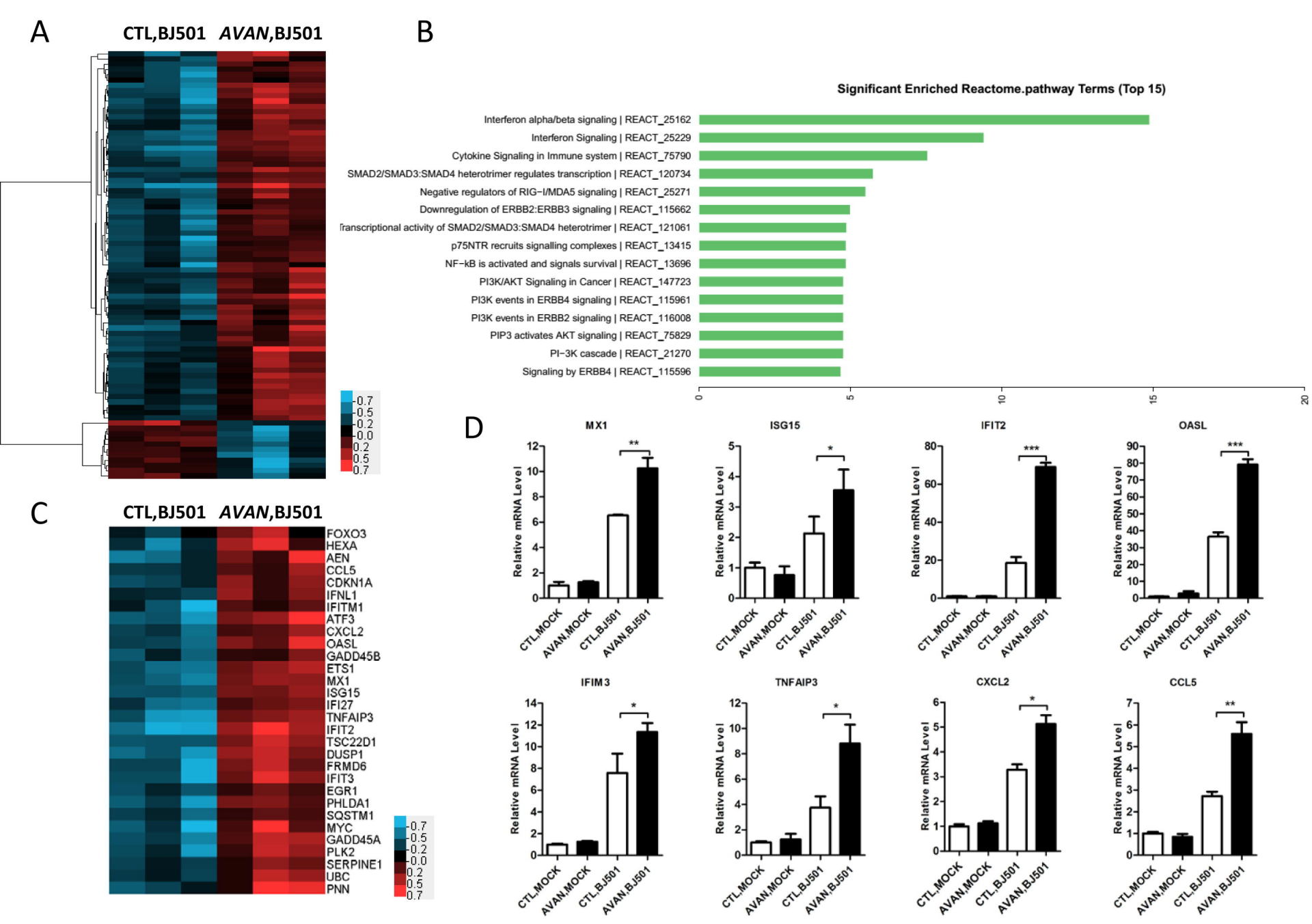
A
CTL,BJ501 AVAN,BJ501
0.7
0.5
0.2
0.0
0.2
0.5
0.7
B
Significant Enriched Reactome.pathway Terms (Top 15)
Interferon alpha/beta signaling | REACT_25162
Interferon Signaling | REACT_25229
Cytokine Signaling in Immune system | REACT_75790
SMAD2/SMAD3:SMAD4 heterotrimer regulates transcription | REACT_120734
Negative regulators of RIG-I/MDA5 signaling | REACT_25271
Downregulation of ERBB2:ERBB3 signaling | REACT_115662
Transcriptional activity of SMAD2/SMAD3:SMAD4 heterotrimer | REACT_121061
p75NTR recruits signalling complexes | REACT_13415
NF-kB is activated and signals survival | REACT_13696
PI3K/AKT Signaling in Cancer | REACT_147723
PI3K events in ERBB4 signaling | REACT_115961
PI3K events in ERBB2 signaling | REACT_116008
PIP3 activates AKT signaling | REACT_75829
PI-3K cascade | REACT_21270
Signaling by ERBB4 | REACT_115596
0
5
10
15
20
C
CTL,BJ501 AVAN,BJ501
FOXO3
HEXA
AEN
CCL5
CDKN1A
IFNL1
IFITM1
ATF3
CXCL2
OASL
GADD45B
ETS1
MX1
ISG15
IFI27
TNFAIP3
IFIT2
TSC22D1
DUSP1
FRMD6
IFIT3
EGR1
PHLDA1
SQSTM1
MYC
GADD45A
PLK2
SERPINE1
UBC
PNN
0.7
0.5
0.2
0.0
0.2
0.5
0.7
D
MX1
ISG15
IFIT2
OASL
IFIM3
TNFAIP3
CXCL2
CCL5
Relative mRNA Level
CTL,MOCK
AVAN,MOCK
CTL,BJ501
AVAN,BJ501

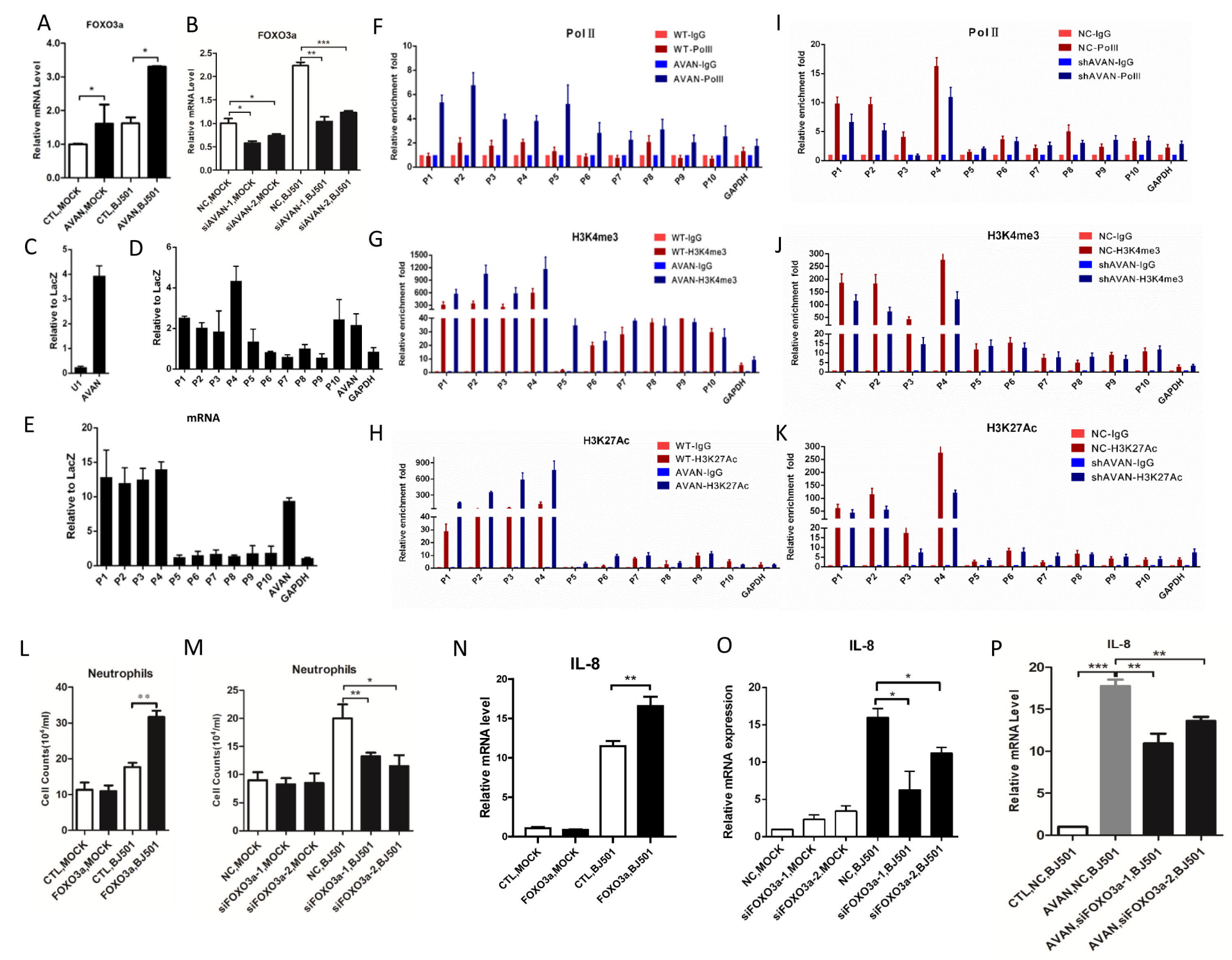
A
FOXO3a
Relative mRNA Level
CTL,MOCK
AVAN,MOCK
CTL,BJ501
AVAN,BJ501
B
FOXO3a
Relative mRNA Level
NC,MOCK
siAVAN-1,MOCK
siAVAN-2,MOCK
NC,BJ501
siAVAN-1,BJ501
siAVAN-2,BJ501
C
Relative to LacZ
U1
AVAN
D
Relative to LacZ
P1 P2 P3 P4 P5 P6 P7 P8 P9 P10 AVAN GAPDH
E
mRNA
Relative to LacZ
P1 P2 P3 P4 P5 P6 P7 P8 P9 P10 AVAN GAPDH
F
PolⅡ
Relative enrichment fold
WT-IgG
WT-PolII
AVAN-IgG
AVAN-PolII
P1 P2 P3 P4 P5 P6 P7 P8 P9 P10 GAPDH
G
H3K4me3
Relative enrichment fold
WT-IgG
WT-H3K4me3
AVAN-IgG
AVAN-H3K4me3
P1 P2 P3 P4 P5 P6 P7 P8 P9 P10 GAPDH
H
H3K27Ac
Relative enrichment fold
WT-IgG
WT-H3K27Ac
AVAN-IgG
AVAN-H3K27Ac
P1 P2 P3 P4 P5 P6 P7 P8 P9 P10 GAPDH
I
PolⅡ
Relative enrichment fold
NC-IgG
NC-PolII
shAVAN-IgG
shAVAN-PolII
P1 P2 P3 P4 P5 P6 P7 P8 P9 P10 GAPDH
J
H3K4me3
Relative enrichment fold
NC-IgG
NC-H3K4me3
shAVAN-IgG
shAVAN-H3K4me3
P1 P2 P3 P4 P5 P6 P7 P8 P9 P10 GAPDH
K
H3K27Ac
Relative enrichment fold
NC-IgG
NC-H3K27Ac
shAVAN-IgG
shAVAN-H3K27Ac
P1 P2 P3 P4 P5 P6 P7 P8 P9 P10 GAPDH
L
Neutrophils
Cell Counts(10^4/ml)
CTL,MOCK
FOXO3a,MOCK
CTL,BJ501
FOXO3a,BJ501
M
Neutrophils
Cell Counts(10^4/ml)
NC,MOCK
siFOXO3a-1,MOCK
siFOXO3a-2,MOCK
NC,BJ501
siFOXO3a-1,BJ501
siFOXO3a-2,BJ501
N
IL-8
Relative mRNA level
CTL,MOCK
FOXO3a,MOCK
CTL,BJ501
FOXO3a,BJ501
O
IL-8
Relative mRNA expression
NC,MOCK
siFOXO3a-1,MOCK
siFOXO3a-2,MOCK
NC,BJ501
siFOXO3a-1,BJ501
siFOXO3a-2,BJ501
P
IL-8
Relative mRNA Level
CTL,NC,BJ501
AVAN,NC,BJ501
AVAN,siFOXO3a-1,BJ501
AVAN,siFOXO3a-2,BJ501

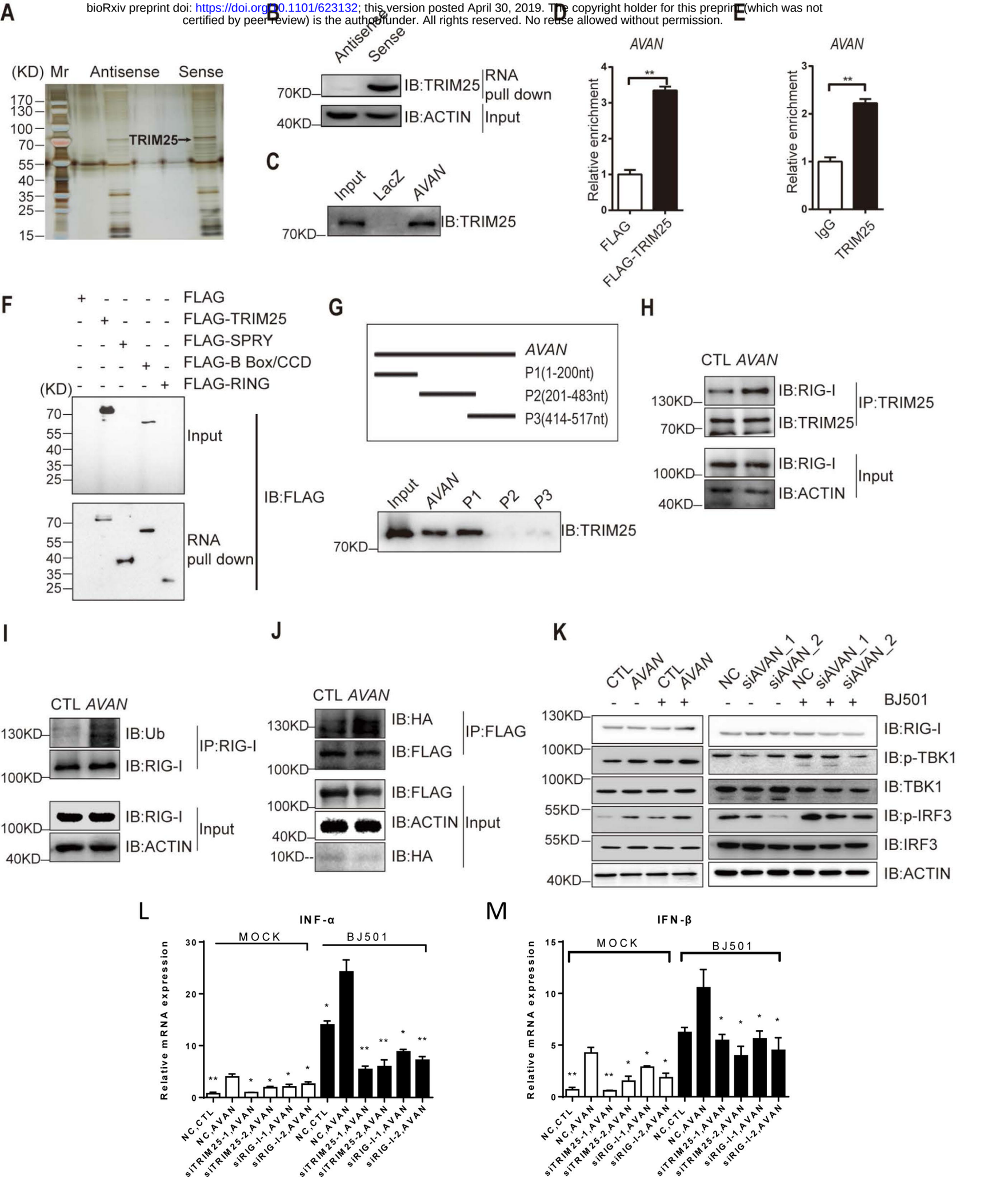

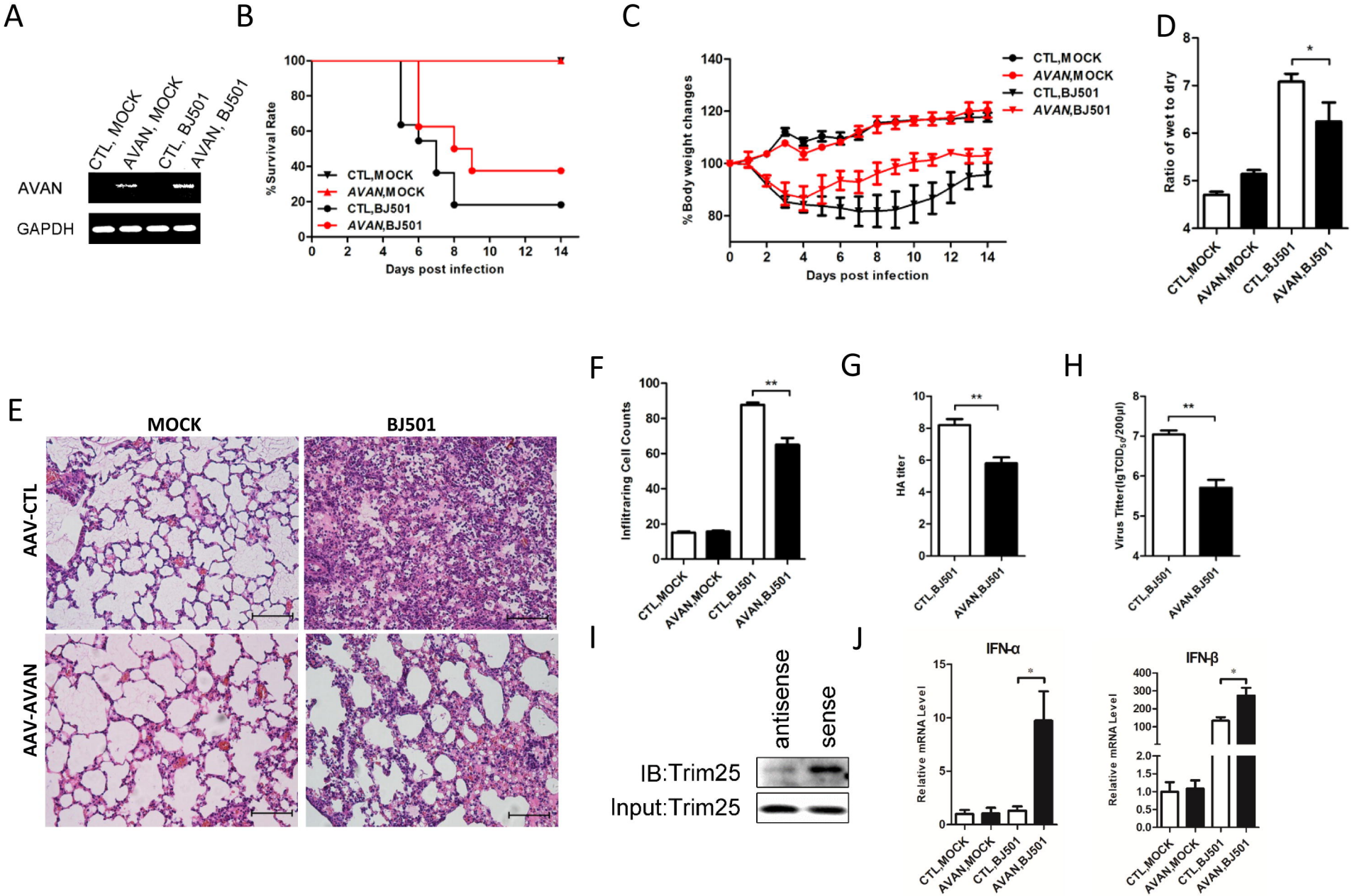
A
CTL, MOCK
AVAN, MOCK
CTL, BJ501
AVAN, BJ501
AVAN
GAPDH
B
% Survival Rate
Days post infection
CTL,MOCK
AVAN,MOCK
CTL,BJ501
AVAN,BJ501
C
% Body weight changes
Days post infection
CTL,MOCK
AVAN,MOCK
CTL,BJ501
AVAN,BJ501
D
Ratio of wet to dry
CTL,MOCK
AVAN,MOCK
CTL,BJ501
AVAN,BJ501
E
MOCK
BJ501
AAV-CTL
AAV-AVAN
F
Infiltrating Cell Counts
CTL,MOCK
AVAN,MOCK
CTL,BJ501
AVAN,BJ501
G
HA titer
CTL,BJ501
AVAN,BJ501
H
Virus Titer(lgTCID50/200μl)
CTL,BJ501
AVAN,BJ501
I
antisense
sense
IB:Trim25
Input:Trim25
J
IFN-α
Relative mRNA Level
CTL,MOCK
AVAN,MOCK
CTL,BJ501
AVAN,BJ501
IFN-β
Relative mRNA Level
CTL,MOCK
AVAN,MOCK
CTL,BJ501
AVAN,BJ501

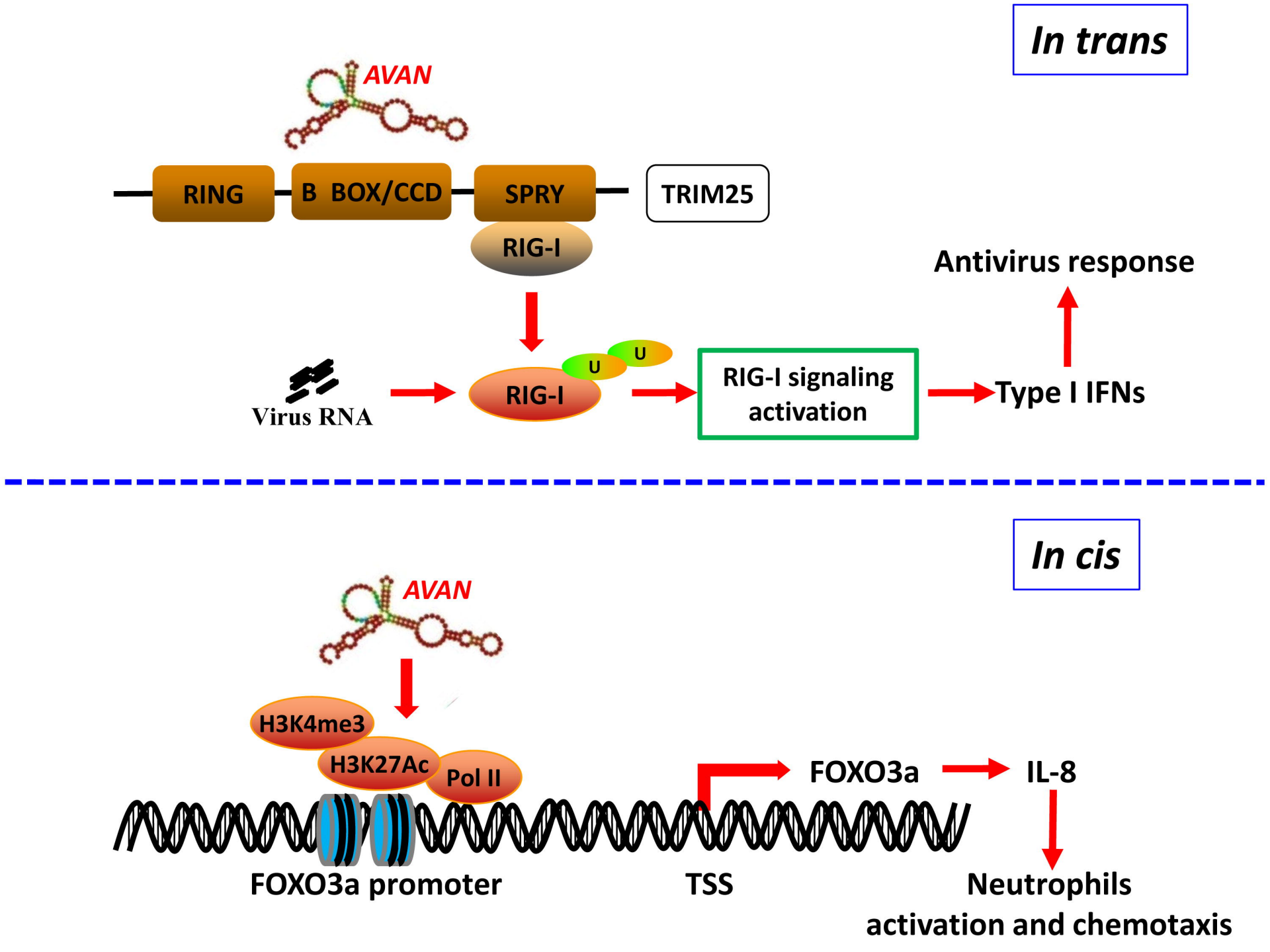
In trans
AVAN
RING
B BOX/CCD
SPRY
TRIM25
RIG-I
Antivirus response
Virus RNA
U
U
RIG-I
RIG-I signaling activation
Type I IFNs
In cis
AVAN
H3K4me3
H3K27Ac
Pol II
FOXO3a
IL-8
FOXO3a promoter
TSS
Neutrophils activation and chemotaxis